IA

COMPTEL

COMPTEL PREPRINTs NO. 20-23

March 1995
Accepted for publication in
Astronomy & Astrophysics

THE COMPTEL COLLABORATION

Max-Planck-Institut für Extraterrestrische Physik, Garching, FRG
SRON-Leiden, Leiden, The Netherlands
Space Science Center, University of New Hampshire, Durham NH, USA
Astrophysics Division, European Space Research and Technology Centre,
Noordwijk, The Netherlands

A&A manuscript no.
(will be inserted by hand later)

Your thesaurus codes are:
missing; you have not inserted them

ASTRONOMY
AND
ASTROPHYSICS
14.3.1995

COMPTEL observations of the Crab during the CGRO sky survey

R. Much[4,1], K. Bennett[4], R. Buccheri[5], M. Busetta[4], R. Diehl[1], D. Forrest[3], W. Hermsen[2], L. Kuiper[2], G.G. Lichti[1], M. McConnell[3], J. Ryan[3], V. Schönfelder[1], H. Steinle[1], A. Strong[1], M. Varendorff[1]

[1] Max Planck Institut für extraterrestrische Physik, P.O. Box 1603, D-85740 Garching, Germany
[2] SRON-Leiden, P.B. 9504, NL-2300 RA Leiden, The Netherlands
[3] University of New Hampshire, Institute for the Study of Earth, Oceans and Space, Durham NH 03824, USA
[4] Astrophysics Division, ESTEC, NL-2200 AG Noordwijk, The Netherlands
[5] IFCAI/CNR, Piazza G. Verdi 6, 90139 Palermo, Italy

March 14, 1995

Abstract. During the all-sky survey of the Compton Gamma Ray Observatory (CGRO) the Crab pulsar and nebula were observed several times. The unprecedented exposure allows detailed spectral shape determination together with a phase-resolved study of the Crab pulsar in the 0.75-30 MeV energy range. We show that, except for the second peak, the phase-resolved COMPTEL data cannot be described by a simple extrapolation of the higher energy (50 MeV-10 GeV) EGRET best-fit power-law. Evidence was found for time variability of the unpulsed emission on a time scale of 16 months.

Key words: Gamma rays: observations – pulsars: general – pulsars: individual: PSR 0531+21 – ISM: Crab Nebula

1. Introduction

The Crab was first reported to be a γ-ray source by Hillier *et al.* (1970). Since then its γ-ray emission, from the MeV to the TeV energy range, has been firmly established by numerous other experiments (e.g. Parlier *et al.* 1973; Graser & Schönfelder 1982; White *et al.* 1985; Clear *et al.* 1987; Jung 1989; Akerlof *et al.* 1990; Vacanti *et al.* 1991; Natalucci *et al.* 1991).

The Crab can be classified as a rotation powered isolated pulsar, with a spinning neutron star in the centre of a nebula emitting a highly energetic pulsar wind (Ho 1993). The unresolved γ-ray emission from the Crab region consists of two components: an unpulsed and a pulsed component. Basically two models exist giving an explanation for the pulsed γ-ray emission of the Crab: the "outer-gap" model (Cheng, Ho & Ruderman 1986a,b; Ho 1989) and the "polar-cap" model (Harding 1981, Daughtery & Harding 1982). A combination of these two models or a modified polar cap model have been recently suggested to account for the production of the pulsed emission by Kamae and Sekimoto (1994) and by Sturner and Dermer (1994) respectively. All these models explain the observed pulsed γ-ray emission by interactions of highly energetic electrons and positrons ($e^{\pm}$) which are accelerated to relativistic energies in the magnetosphere of the pulsar. They differ in the location where this acceleration of the primary $e^{\pm}$ takes place.

A large proportion of the Crab pulsar's loss of rotational energy is observed in the unpulsed emission. While γ-ray instruments cannot resolve the Crab pulsar from the Crab nebula, measurements from radio to X-rays are able to resolve the Crab nebula. At X-ray energies (0.1-4.5 keV) Harnden and Seward (1984) have shown that the pulsed flux originates within the instrument resolution at the position of the pulsar. They reported that the pulsed emission decreases to zero over roughly an eighth of the pulsar period, the so called "off"-phase interval. So, assuming no pulsed emission in the "off" phase interval at γ-ray energies, it is possible to disentangle pulsed and unpulsed emission via phase selection.

Polarization measurements from radio to X-ray energies indicate that the unpulsed continuum is synchrotron radiation. High energy particles supplied by the pulsar wind synchrotron radiate while gyrating in the magnetic field of the nebula (Kennel & Coroniti 1984). The smooth fit between the X-ray and γ-ray spectrum suggests that the unpulsed continuum also in the γ-ray range originates from synchrotron radiation.

De Jager and Harding (1992) extended this model in order to explain the observed unpulsed TeV emission (Weekes

Send offprint requests to: R. Much (Astrophysics Division, ESTEC)

et al. 1989, Vacanti *et al.* 1991). They suggested that electrons of the pulsar wind are reaccelerated in a shock front up to energies of 10^{16} eV, thus being able to boost soft photons to TeV energies via inverse Compton scattering.
A new aspect of the Crab unpulsed emission is the claimed time variability discovered by EGRET (De Jager *et al.* 1993, 1994). De Jager *et al.* associate this time variability with an unstable electron acceleration at the pulsar wind shock.
The present paper reports the results from COMPTEL, the medium energy range experiment (0.75-30 MeV) aboard CGRO, of the Crab observations during the CGRO sky survey, also known as CGRO Phase I. A preliminary analysis of parts of the data used here has been given by Strong *et al.* (1993).

2. Instrumentation and Observations

COMPTEL is a Compton telescope consisting of two scintillator detector planes separated by ~ 1.50 m. Ideally, a photon is detected by a Compton scatter in the upper detector with subsequent total absorption in the lower detector. From the measured energy deposits of the photon in the two detectors (E_1 and E_2) and from the kinematics of the Compton scattering process, the scatter angle in the upper detector can be calculated:

$$\cos\bar{\varphi} = 1 - \frac{m_e c^2}{E_2} + \frac{m_e c^2}{E_1 + E_2} \qquad \text{with } m_e c^2 = 511\,\text{keV}. \quad (1)$$

Using the Anger camera principle the photon interaction can be localized both in the upper and lower detector plane (Connors *et al.* 1992). This determines the scatter direction of the photon (χ, ψ). In the ideal case the incoming direction of a photon is known to lie somewhere on a projected circle on the sky, the so-called *event circle*, with a centre at (χ, ψ) and with radius $\bar{\varphi}$. It needs the interpretation of many events to localize a source. The scatter direction angles (χ, ψ) and the derived scatter angle $\bar{\varphi}$ constitute a 3-dimensional data space. The signature of a point source in this data space is cone-shaped (Diehl *et al.* 1992). Recognition of source signature in the 3-dimensional data space using, for example, maximum likelihood ratio techniques (de Boer *et al.* 1992) makes it possible to localize a source. A full description of the COMPTEL instrument is given by Schönfelder *et al.* (1993).

In May 1991 the first 0.75-30 MeV all-sky survey in the history of γ-ray astronomy was started by COMPTEL, and was completed in November 1992. The galactic anticentre region including the Crab was within 25° of the instrument z-axis on five separate occasions during this survey period. This was the case during the validation period, in the following called observation 0, and the observations 1, 2.5, 36 and 39. Data from observation 0 were used to verify the proper functioning of the instrument and to optimize the onboard data selections. Since the actual validation activities of COMPTEL were finished earlier than anticipated (28^{th} April, 1992), the data collected during the later part of the validation period could be used for scientific analysis. Observation 2.5 was a target-of-opportunity observation of the active Sun. During this time, the onboard data selections were modified so as to optimize the efficiency for collecting data during solar flares. These data cannot be combined with the data when the instrument is in normal mode because the change in the data selections of the solar observation mode also modifies the instrument response. Therefore the data of observation 2.5 are not included here. The details of the remaining four observations are summarized in Table 1. For the present analysis identical data selections and software cuts are applied to the data of the different observation periods. Software cuts are chosen conservatively so as to exclude a possible impact of a change of the hardware thresholds on the data analysis. The effective exposure, which is energy dependant (cf. Schönfelder *et al.* 1993), is specified for the energy interval 1 to 3 MeV in Table 1. Although during the validation period (observation 0) and observation 36 the pointing directions were changed, these periods are treated as one observation in the present analysis. Note that the amount of scientifically usable data of the validation period is different for the different CGRO instruments, e.g. EGRET Crab data are used starting with 23^{rd} April, 1992 (Nolan *et al.* 1993).

3. Timing Analysis

3.1. Method

The timing analysis was performed with the pulsar analysis subsystem (PUL) of the COMPTEL processing and analysis software system (COMPASS) (Busetta *et al.* 1992). The COMPTEL clock has a resolution of 1/8 ms which is sufficient for timing analysis of all known pulsars. During the early CGRO mission an absolute error of the CGRO clock of 2.0421 s was found. This error was corrected for and does not affect the present analysis. With the current analysis system absolute timing is achieved to a level of ~ 0.5 ms. The issue of a possible phase shift between radio pulse and γ-ray peak of the order of $\sim 500\mu s$ as reported by Masnou *et al.* (1994) cannot be addressed. In addition to the standard filtering of the raw data, e.g. time of flight or pulse shape window (cf. Schönfelder *et al.* 1993), the data are selected on the basis of the distance of the *event circle* from the source position of interest, the so called "ARM cut". An event is only used in the timing analysis when its *event circle* passes within 3° of the source position.
Ephemerides of contemporaneous Crab radio observations listed in Table 2 were used to fold the data once the photon arrival times were transformed to Solar System Barycen-

Obs. #	T_{start} dd-mm-yy	T_{end} dd-mm-yy	Pointing l (°)	Pointing b (°)	Crab View Angle	Exposure (10^6 s·cm^2)
0.5	28-04-91	01-05-91	193.4	-4.3	8.9°	2.52
0.4	01-05-91	04-05-91	193.4	-4.3	8.9° *	2.33
0.3	04-05-91	07-05-91	184.5	-5.9	0.1°	2.66
1.0	16-05-91	30-05-91	191.0	-4.6	6.5°	8.52
36.0	11-08-92	12-08-92	169.8	-11.4	15.6°	0.68
36.5	12-08-92	20-08-92	168.2	-9.5	16.7°	3.12
39.0	01-09-92	17-09-92	167.2	-9.2	17.6°	4.78

*compared to observation 0.5 the spacecraft was rotated by 90° in azimuthal direction

Table 1. COMPTEL observations of the Crab used in the present work.

Obs. #	T_0	f (s^{-1})	$\dot{f}$ ($s \cdot s^{-1}$)	$\ddot{f}$ ($s \cdot s^{-2}$)
0.	48367	29.9493820573442	-3.77660D-10	7.45D-21
1.	48367	29.9493820573442	-3.77660D-10	7.45D-21
36	48824	29.9344793547924	-3.77193D-10	1.45D-20
39.0	48881	29.9326219100202	-3.77130D-10	1.40D-20

Table 2. Contemporary radio ephemerides (Arzoumanian et al. 1992) used in the timing analysis. The position of the Crab used is α=5h 34' 31.973", δ= 22° 00' 52.06".

tre. In this way light curves for preselected energy intervals were constructed by phase binning for the single observations as well as for the combined observations. The entire pulsar cycle was first divided into two intervals: an off- and an on-phase interval. The on-phase interval was further subdivided adopting the definitions given by Nolan *et al.* (1993), which allows a direct comparison with the EGRET results. These phase interval definitions are listed in Table 3 and are indicated in Fig. 1.

Region	Symbol	Phase Interval
First Pulse	P_1	0.915-0.045
Interpulse 1	I_1	0.045-0.215
Interpulse 2	I_2	0.215-0.315
Second pulse	P_2	0.315-0.445
Trailer	T	0.445-0.525
Total pulse	P_{tot}	0.915-0.525
Off-phase	off	0.525-0.915

Table 3. Used definition of phase intervals for the Crab pulsar light curve (after Nolan *et al.* 1993)

3.2. Results of Timing Analysis

Carramiñana *et al.* (1994) have shown that no statistically significant differences can be found between the shapes of the light curves measured with COMPTEL for different observation periods. Therefore in order to improve statistics, we have combined the light curves for the different observation periods in this analysis.

A statistically significant signal from the Crab pulsar is seen by COMPTEL only in the energy range 0.75-10 MeV. The Crab light curve for the combined observations in this energy interval is shown in Fig. 1.

The light curve has a structure which is similar to that measured in adjacent energy intervals (Clear *et al.* 1987; Agrinier *et al.* 1990; Nolan *et al.* 1993): two peaks separated by 0.42 in phase, an interpulse region between the peaks and an off-region with no pulsed emission. However, the interpulse emission exhibited in the 0.75 to 10 MeV range is proportionally considerably larger than in the energy range above 50 MeV (Nolan *et al.* 1993) and is comparable to the structure shown at hard X-rays (Ulmer *et al.* 1994; Buccheri *et al.* 1994).

An independent search for the definition of the pulsed phase intervals was performed in the COMPTEL light curve to check the compatibility with the EGRET phase definitions. The pulsed region of the light curve was determined by searching for the maximum deviation from a flat distribution of the events. The χ^2 was maximized in respect to the location and width of the pulsed interval. The derived pulsed region extends from 0.915 to 0.445 in the COMPTEL light curve, stretching from the beginning of the first peak to the end of the second peak. With this method, no significant pulsed emission was found in the trailer region, although in Fig. 1 a shoulder seems to be present. The χ^2 obtained applying the EGRET definitions

P_2/P_1 Ratios	Energy Interval (MeV)				
Observation	0.75-1.0	1.0-3.0	3.0 -10	1. - 10.	> 50 (EGRET)
0	-	1.26±0.34	1.26±0.52	1.26±0.28	0.45±0.05
1	1.77±1.33	1.47±0.37	-	1.26±0.30	0.52±0.06
36	-	2.15±1.09	-	-	-
39	-	1.32±0.41	-	2.04±0.77	-
all	3.01±1.48	1.58±0.25	1.61±0.68	1.49±0.22	-

Table 4. Ratio of second to first peak background subtracted counts in the Crab light curve for different energy intervals and observations. The ratio is only derived for the COMPTEL data if the count excess in both phase intervals, P_1 and P_2 is greater than 2σ. The ratios above 50 MeV of observation 0 and 1 are taken from Nolan *et al.* (1993).

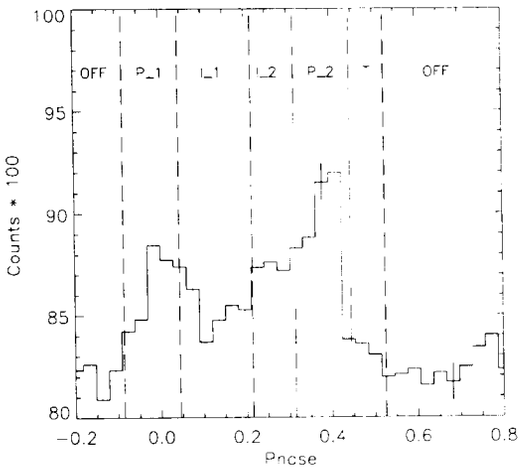

Fig. 1. The 33-bin Crab light curve for the energy interval 0.75-10 MeV. Only in this energy interval is a statistically significant signal of the Crab pulsar seen by COMPTEL. Indicated are the $\pm 1\sigma$ error bars. The phase intervals adopted from Nolan *et al.* (1993) are marked with dashed lines. Note that the zero count level is suppressed.

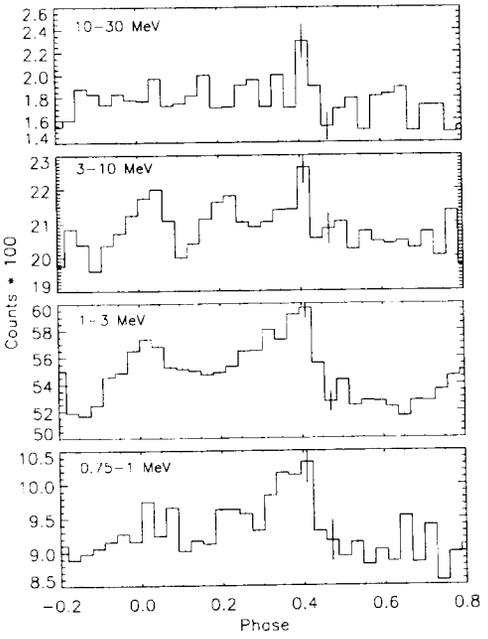

Fig. 2. The 33-bin Crab light curves for the four COMPTEL standard energy intervals for the combined observations of Phase I. Indicated are the $\pm 1\sigma$ error bars.

(0.915 to 0.525 in phase) to the COMPTEL light curve is within statistical uncertainty compatible with the optimal definitions of the pulsed phase interval. Therefore we could adopt the EGRET definitions for our analysis.

Light curves were also created for four energy bands which are routinely used in the COMPTEL data analysis, namely 0.75-1.0 MeV, 1.0-3.0 MeV, 3.0-10 MeV and 10-30 MeV. The resulting light curves are shown in Fig. 2. In the energy interval 10-30 MeV no significant pulsed emission was found with the timing analysis, which is to be expected given the COMPTEL sensitivity and the relatively soft spectrum of the Crab pulsar.

After subtraction of the background level, determined in the off-phase interval, the excess counts in the P_1-phase interval can be determined and compared to the excess counts in the P_2-phase interval. This is done for the three low energy bands, in which the pulsed emission is significant, and in the 1 to 10 MeV energy interval where we obtain the best signal-to-noise ratio. In some cases the significance of the count excess of the first peak is too low, so that we cannot determine the ratio. Table 4 summarizes the numbers resulting from our analysis and shows also the ratios reported by Nolan *et al.* 1993 for energies above 50 MeV.

In the COMPTEL data there are no indications for a variation of the P_2/P_1 ratio between the single observations as reported by Nolan *et al.* (1993). The change in the ratio reported by Nolan *et al.* is consistent with the sinusoidal variation with a period of 13.5 years, which was determined by Kanbach (1990) using COS-B and SAS 2 data. Within their 1σ uncertainty the COMPTEL ratios are constant. The large uncertainties are due to the low signal-to-noise ratio in the light curve.

A comparison with the EGRET (Nolan *et al.* 1993) and OSSE (Ulmer *et al.* 1994) results shows that the COMPTEL values are systematically greater than the EGRET ones. OSSE derived their P_2/P_1 values in the 50-340 keV energy band. Their ratios ($\sim$ 1.4) are statistically consistent with the ratios of COMPTEL, although Ulmer *et al.* (1994) used slightly different phase definitions. A detailed comparison with the other CGRO experiments using consistent phase definitions for all instruments will be provided by Ulmer *et al.* (1995).

4. Spectral Analysis

4.1. Method

A maximum entropy or a maximum likelihood method is used to search for the signature of point sources in this 3-dimensional dataspace as described by Strong *et al.* (1992) and de Boer *et al.* (1992) respectively. The maximum likelihood method simultaneously determines photon fluxes along with the associated statistical errors. The required background model for the likelihood analysis was calculated from the measured photon distribution in the 3-D dataspace itself by applying a filtering technique (Bloemen *et al.* 1993).

A maximum entropy and maximum likelihood map of the Crab region for the off-pulse phase between 10 and 30 MeV are shown in Fig. 3. The observations listed in Table 1 were combined when generating these maps. The deconvolution inherent in the maximum entropy method results in a narrower peak at the position of the Crab compared to the peak in the maximum likelihood map. The Crab is the only statistically significant ($> 3\sigma$) feature in this likelihood map of the phase selected data.

COMPTEL's spatial resolution is not sufficient to resolve the Crab pulsar from the surrounding nebula. In order to separate the pulsed and unpulsed emission the commonly used convention in γ-ray astronomy is applied (Clear *et al.* 1987; Nolan *et al.* 1993): it is assumed that the pulsed emission does not contribute to the emission in the off-pulse phase and the unpulsed emission remains constant over the full pulsar period. The unpulsed emission can therefore be determined by selecting only events detected in the off-pulse phase defined in Table 3 (see also Fig. 1). Once the unpulsed flux $\Phi_{\Delta_{up}}$ is known, the pulsed photon flux Φ_{Δ_p} of a specific phase interval Δ_p is derived from the total photon flux $(\Phi_{total})_{\Delta_p}$ by subtracting the component of the unpulsed emission:

$$\Phi_{\Delta_p} = (\Phi_{total})_{\Delta_p} - \Phi_{\Delta_{up}} \cdot \frac{\Delta_p}{\Delta_{up}} \qquad (2)$$

where Δ_p/Δ_{up} is the ratio of the width of the pulsed phase to the width of the unpulsed phase interval.

4.2. Unpulsed Emission

For the standard energy intervals the unpulsed photon fluxes of the individual observations are listed in Table 5. The fluxes are normalized to the full period though they are determined in the phase interval 0.525-0.915 (= 0.39 of total phase).

Obs. #	unpulsed photon fluxes (10^{-4} photons / (cm^2 · s)) 0.75-1 MeV	1-3 MeV	3-10 MeV	10-30 MeV
0.	4.49±0.98	9.42±1.01	3.37±0.47	0.61±0.19
1.0	4.10±0.95	6.97±0.97	3.42±0.46	0.88±0.18
36	5.64±1.25	9.14±1.37	4.76±0.69	<1.04
39.0	6.63±1.08	11.13±1.18	4.81±0.60	1.68±0.31

Table 5. Crab unpulsed fluxes for the standard energy intervals. The quoted errors are statistical only. Errors are 1σ, upper limit 2σ.

For the further analysis we have combined the data of observation 0 with 1 and observation 36 with 39 for three reasons, first to improve statistics, second because there is no significant variation ($< 2\sigma$) between each of the two observations and finally the combined observations are only separated by a short time period. The combination of two COMPTEL observations provides sufficient statistics to split the 1-10 MeV range into finer energy bins. The energy intervals have been chosen in such a way that the number of events in the different energy bins are of the same order. A $\pm 1\sigma$ energy window around the instrumental 2.23 MeV line originating in neutron capture processes of ^{12}C in the D1-detector material (Schönfelder *et al.* 1993) has been excluded from this analysis when the finer energy binning was used. This was done to avoid a possible distortion of the flux calculation by the instrumental line, which may occur in case of low statistics. The chosen energy intervals and the corresponding fluxes are listed in Table 6.

Energy range (MeV)	unpulsed photon fluxes (10^{-4} photons / (cm^2 · s)) Obs. # 0+1	Obs. # 36+39
0.75-1.0	4.52±0.69	6.31±0.82
1.0-1.6	4.67±0.57	5.82±0.70
1.6-2.1	2.14±0.33	2.18±0.42
2.36-4.0	2.23±0.32	3.46±0.42
4.0-5.6	1.04±0.17	1.53±0.25
5.6-10.0	0.97±0.16	1.60±0.24
10-30	0.83±0.13	1.15±0.22

Table 6. Crab unpulsed fluxes of the combined observations 0+1 and 36+39

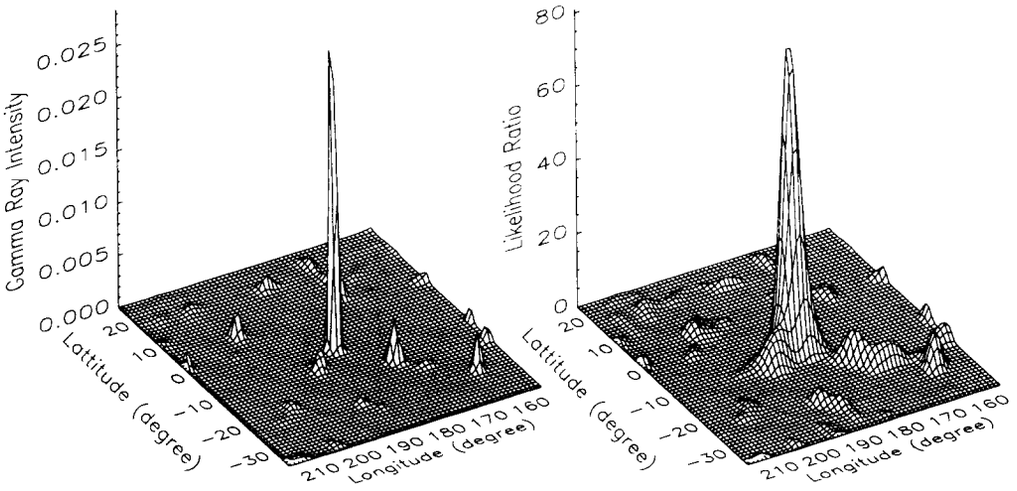

Fig. 3. The maximum entropy (left) and maximum likelihood map (right) of the Crab region for the off-pulse phase between 10 and 30 MeV. Any structure other than the Crab is statistically insignificant.

We achieved a good fit to spectra of the combined observations in both cases with a simple power-law. The fits (5 degree of freedom) resulted with an unreduced χ^2 of 1.15 (observation 0+1) and 4.64 (observation 36+39) in:

$$(d\Phi_{up}/dE)_{0+1} = (1.93\pm0.17)\cdot10^{-4}\cdot(\frac{E_{MeV}}{2.6})^{-(2.02\pm0.09)} \quad (3)$$

$$(d\Phi_{up}/dE)_{36+39} = (2.65\pm0.22)\cdot10^{-4}\cdot(\frac{E_{MeV}}{2.6})^{-(1.94\pm0.09)} \quad (4)$$

The energy scaling constant of 2.6 MeV is chosen to give uncorrelated errors on intensity and spectral index of the power-law. Following Lampton *et al.* (1976) we estimated the 1σ errors of the fit parameters by increasing χ^2_{min} by 2.3.

The unpulsed spectra for the two combined observations are represented as a power-per-decade diagram in Fig. 4 together with measurements from GRIS (Bartlett *et al.* 1993) and EGRET (Nolan *et al.* 1993). The GRIS data are shown as 2σ upper limits if the measured flux has a significance of less than 2σ.

From Table 6 and Fig. 4 we see that in all energy bands the unpulsed fluxes of observations 0+1 in April/May 1991 are lower than these of observations 36+39 in August/September 1992. In order to determine the significance of this variation we had first to consider systematic uncertainties, e.g. impact of data filtering on the result. So far we have found no indication for a change in the COMPTEL sensitivity between different observations. The absolute calibration uncertainty, which is conservatively estimated to be 30 %, does not affect the observed relative flux change.

We quantify the variation in flux between observation 0+1 and 36+39 employing a method used by Worrall (1990) and Worrall and Wilkes (1990), thus we can make use of the finer energy binning. The ratios r_i of the unpulsed fluxes in observation 0+1 and 36+39 and their 1σ uncertainties σ_{r_i} are listed in Table 7. Following Worrall we determined the mean flux ratio $\bar{r}$ together with the intrinsic dispersion of the flux ratios $\sigma_{\bar{r}}$ by minimizing the function S (equ. 5). S is distributed as χ^2 with 2 degree of freedom in respect to the variables $\bar{r}$ and $\sigma_{\bar{r}}$.

$$S = \sum_i [\frac{(r_i - \bar{r})^2}{\sigma^2_{\bar{r}} + \sigma^2_{r_i}} + ln(\sigma^2_{\bar{r}} + \sigma^2_{r_i})] \quad (5)$$

The intrinsic dispersion $\sigma_{\bar{r}}$ is in our case a measure of the energy dependence of the flux ratio $\bar{r}$. We obtained an mean ratio of $\bar{r} = 0.72\pm0.09$ and an intrinsic dispersion of the ratio distribution $\sigma_{\bar{r}} = 0.00\pm0.12$. The increase in flux from observation 0+1 to 36+39 by 0.72 has a probability of $1.2\ 10^{-3}$ being a random fluctuation. The zero intrinsic dispersion $\sigma_{\bar{r}}$ indicates that our data are consistent with an energy independence of the flux change.

4.3. Pulsed Emission

The phase interval 0.915 to 0.525 was used to determine the phase-averaged pulsed emission. Although only a hint for pulsed emission was found by the COMPTEL timing analysis within the trailer phase, this sub-interval was included to permit a direct comparison with the total pulsed flux reported by Nolan *et al.* 1993. The exclusion of the

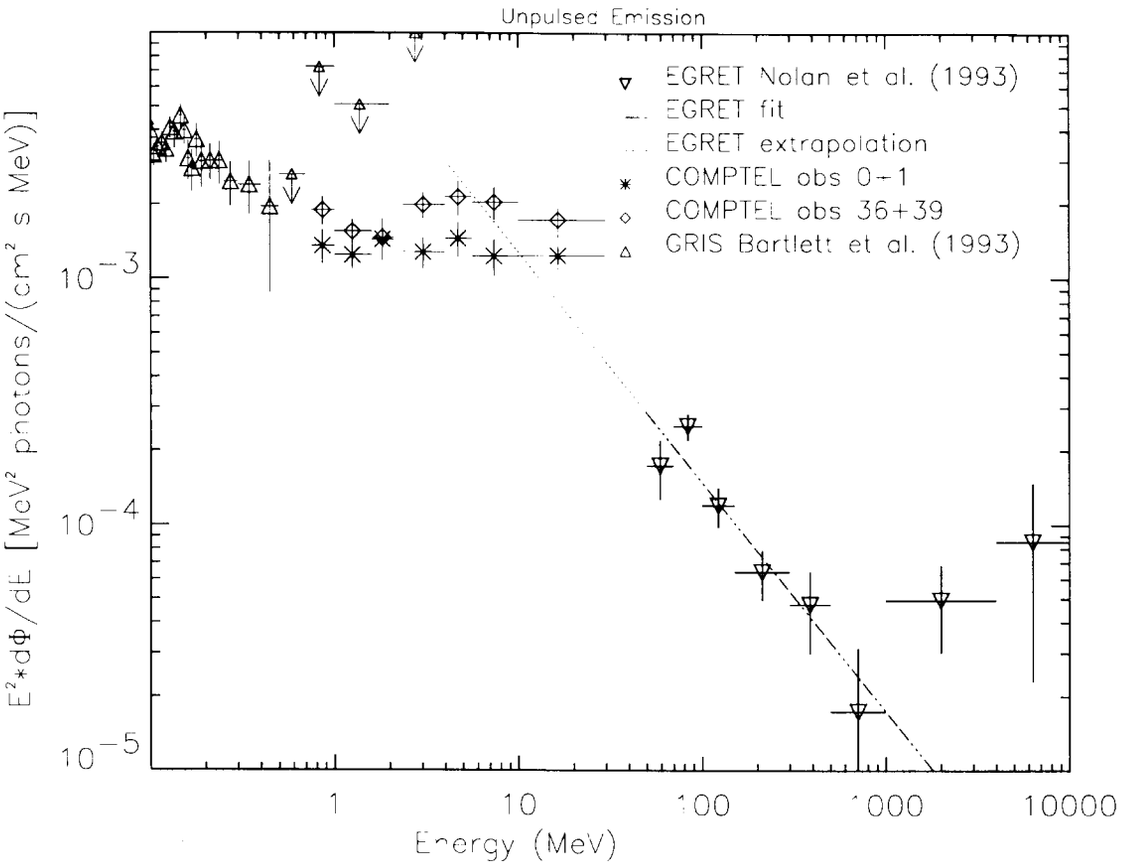

Fig. 4. Spectrum of the unpulsed Crab emission. The COMPTEL data displayed are for the combination of observation (0+1) and (36+39). The best power-law fit to the EGRET data (dashed dotted) and its extrapolation (dotted) are also shown. The low energy data points are taken from Bartlett *et al.* (1993).

Energy (MeV)	ratio of unpulsed photon fluxes $\Phi_{(0+1)}/\Phi(36+39)$
.75-1.0	0.72 ± 0.15
1.0-1.6	0.80 ± 0.14
1.6-2.1	0.98 ± 0.24
2.36-4.0	0.64 ± 0.12
4.0-5.6	0.68 ± 0.16
5.6-10.	0.61 ± 0.14
10-30	0.72 ± 0.18

Table 7. Ratio of Crab unpulsed fluxes of the combined observations 0+1 and 36+39.

trailer region in the spectral analysis changed the total pulsed flux only marginally.

The phase-averaged pulsed photon flux in the four energy bands was calculated for every observation period listed in Table 1 and for the composite of these observations. The phase-averaged fluxes are summarized in Table 8. The instantaneous photon fluxes (i. e. flux per phase interval) can be obtained by dividing by the width of the phase interval, which is 0.61 in this case. In observation 0 the pulsed emission is detected in all four standard energy bands. Due to the lower exposure in observation 36 and 39 only upper limits can be derived in two or more energy bands. We quote an upper limit, if the detected pulsed flux has a significance of less than 2σ. There is no indication for a time variability of the pulsed emission in any of the four energy bands ($< 2\sigma$).

Obs.	phase-averaged pulsed photon fluxes ($10^{-4}\cdot$ photons / (cm$^2\cdot$ s))			
#	0.75-1 MeV	1-3 MeV	3-10 MeV	10-30 MeV
0.	1.70±0.77	2.50±0.80	0.84±0.37	0.43±0.15
1.0	< 2.97	4.33±0.77	0.75±0.36	< 0.28
36	< 3.65	2.77±1.08	< 1.10	0.53±0.25
39.0	< 2.15	2.39±0.93	< 1.60	< 0.48
sum	1.29±0.42	3.27±0.44	0.61±0.21	0.16±0.09

Table 8. Phase-averaged pulsed flux in the energy bands shown. Quoted errors (1σ) are statistical only. Upper limits are 2σ.

When we combine the four Crab observations we ob-

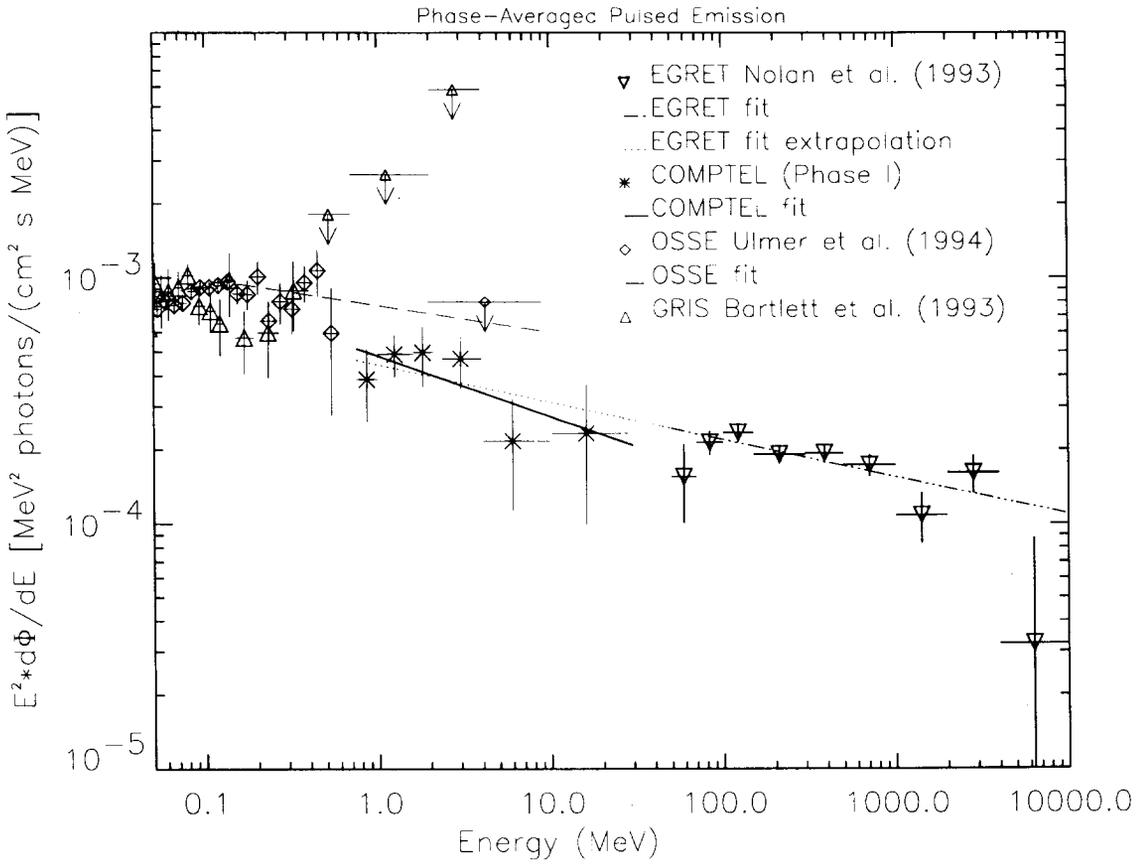

Fig. 5. The phase-averaged photon spectra for the total pulsed emission of the combined Crab observations. GRIS (Bartlett *et al.* 1993), OSSE (Ulmer *et al.* 1994) and EGRET (Nolan *et al.* 1993) results are also displayed.

tain sufficient statistics to use a finer energy binning as described above in the analysis of the unpulsed emission. However, unlike the analysis of the unpulsed emission, we can only split the 1-10 MeV range into four energy intervals, since, due to the lower fluxes of the pulsed emission, the two energy intervals between 4 and 10 MeV have to be merged to render a significant signal. These phase-averaged pulsed fluxes are listed in Table 9. A single power-law fit to the COMPTEL pulsed energy spectrum for the combined Crab observations results in a χ^2_{min} of 2.9 for 4 degrees of freedom. The phase-averaged differential pulsed spectrum for the combined Crab observations is well described by the power-law

$$d\Phi_p/dE = (1.56 \pm 0.29) \cdot 10^{-4} \cdot (\frac{E_{MeV}}{1.65})^{-(2.25 \pm 0.23)} \quad (6)$$

$$(\text{photons}/(\text{cm}^2 \cdot \text{s} \cdot \text{MeV}))$$

The energy scaling constant of 1.65 MeV was chosen to give uncorrelated errors on intensity and spectral index of the power-law. Following Lampton *et al.* (1976) we estimated the 1σ errors of the fit parameters by increasing χ^2_{min} by 2.3.

Within its uncertainty the spectral index of -2.25 is in agreement with the slope of the spectrum above 118 keV (-2.25) measured by OSSE (Ulmer *et al.* 1994) and the slope above 50 MeV (-2.15) as measured by EGRET (Nolan *et al.* 1993). The GRIS, OSSE, EGRET and COMPTEL data are displayed in Fig. 5, where the differential fluxes have been multiplied by E^2. The results of the power-law fits to the OSSE, EGRET and COMPTEL data are also shown. Although the OSSE phase definitions of the pulsed phase interval (0.95-0.65) differ slightly from the EGRET/COMPTEL definitions, the fluxes of the three instruments can nevertheless be compared because the contribution outside the on-phase interval to the total pulsed

Energy range (MeV)	phase-averaged pulsed photon fluxes (photons / (cm^2· s))
1.0-1.6	(1.83±0.35) ·10^{-4}
1.6-2.1	(0.75±0.20) ·10^{-4}
2.36-4.0	(0.82±0.20) ·10^{-4}
4.0-10.	(0.33±0.16) ·10^{-4}

Table 9. Phase-averaged fluxes of the pulsed emission for the combined Crab observations. Supplied 1σ errors are only statistical.

emission is insignificant.
From the values in Tables 5, 6, 8 and 9 the phase-averaged pulsed emission as a fraction of the total (i.e. pulsed plus unpulsed) Crab emission f_P can be derived:

$$f_P = \frac{\Phi_p}{\Phi_p + \Phi_{up}} \tag{7}$$

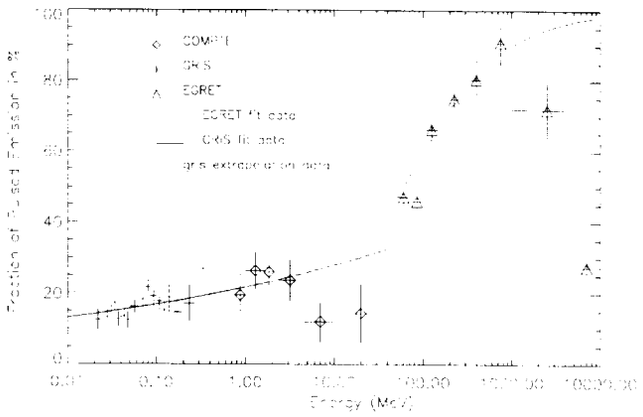

Fig. 6. The fraction of pulsed emission f_P compared with the total emission as a function of energy.

The fraction of pulsed emission is of the order of 20 % in the COMPTEL energy range. At higher energies, between 50 and 500 MeV, a fraction of (47±12)% was reported by Clear *et al.* (1987). At TeV energies the measurements of the Whipple Observatory (Vacanti *et al.* 1991) only supplied upper limits for the pulsed emission - and therefore also on the pulsed fraction.
The energy dependence of the pulsed fraction is displayed in Fig. 6 from 10 keV to 10 GeV. The COMPTEL fractions shown are the average fraction over the four Phase I observations. The datapoints between 20 keV and 300 keV are compiled from the GRIS measurements (Bartlett *et al.* 1993) and between 50 MeV and 10 GeV from the EGRET measurements (Nolan *et al.* 1993). Overlayed are the fractions derived from the power-law fits to the EGRET and GRIS data. There is indication for a dip of the pulsed fraction for energies between 4 MeV and ~30 MeV. This dip results from the monotonic fall off of the unpulsed flux (Fig. 4) and the dip of the pulsed emission between 4 MeV and 30 MeV (Fig. 5). Above 1 GeV the measured fractions drops below the pulsed fraction calculated from the fitted power-laws, because there is indication (2σ) for a increase of the unpulsed Crab emission above 2 GeV (Nolan *et al.* 1993).
For completness it should be noted that we could only derive an upper limit for the pulsed emission in the interval 4 to 5.6 MeV. This is consistent with the lack of excess counts in the light curve. In order to distinguish whether this is a real effect or a result of the sensitivity limit of COMPTEL, further Crab observations have to be added.

4.4. Phase-Resolved Analysis

For the composite of all four observations the achieved source signal was sufficient, from a statistical point of view, to permit the calculation of phase-resolved energy spectra. In Fig. 7a-e the differential instantaneous fluxes (i.e. flux per phase interval) of the phase-resolved analysis are shown. The values are multiplied by E^2.
Although in the majority of cases the COMPTEL data themselves cannot be used to determine the spectral slope of the phase-resolved spectra, they can be used together with the EGRET data to constrain the spectral behaviour. Alone, the spectrum of the second peak (Fig. 7d) can be described with a simple power-law from the low MeV- to the GeV-range. As we obtained a significant detection in three energy intervals, a power-law fit can be made to the COMPTEL data yielding χ^2_{min}=0.8 (2 degrees of freedom). The resulting spectral index $\alpha = 2.27 \pm 0.24$ agrees within its 1σ uncertainty with the EGRET result $\alpha = 2.25 \pm 0.06$ given by Nolan *et al.* (1993).
The spectrum of the first interpulse (Fig. 7b) is consistent with a simple power-law from 1 MeV to 1 GeV, though it requires a spectral slope different from the EGRET best fit slope. The last EGRET data point gives some evidence for a change in spectral shape above 1 GeV. For the other three phase-resolved spectra, first peak, second interpulse and trailer, it can be concluded from the COMPTEL data that the EGRET power-law does not continue into the COMPTEL energy range. This can be seen in Fig. 7 from the extrapolation of the power-laws (with fit parameters at the edge of the 1σ fit uncertainty).
In order to determine the spectral behaviour it is necessary to study it over a wide energy range. This requires that the results from other energy bands be analysed with the same phase definitions. Such an analysis is currently being carried out by the CGRO teams. The differences in phase definitions used by other authors (e.g. Bartlett *et al.* 1993) severely limit a comparison of our results to already existing results, because phase-resolved fluxes are affected by the choice of the phase interval.

5. Discussion

5.1. Unpulsed Emission

Although the Crab Nebula is the most studied plerion, the sensitivity of COMPTEL provided indication of a new feature at low MeV energies, namely the time variability of the γ-ray emission. This was also reported recently by the EGRET team (De Jager and Nel, 1994) for higher γ-ray energies.
The class of relativistic magnetohydrodynamic (MHD) models are currently the most successful in describing the unpulsed emission (Kennel & Coroniti 1984; De Jager

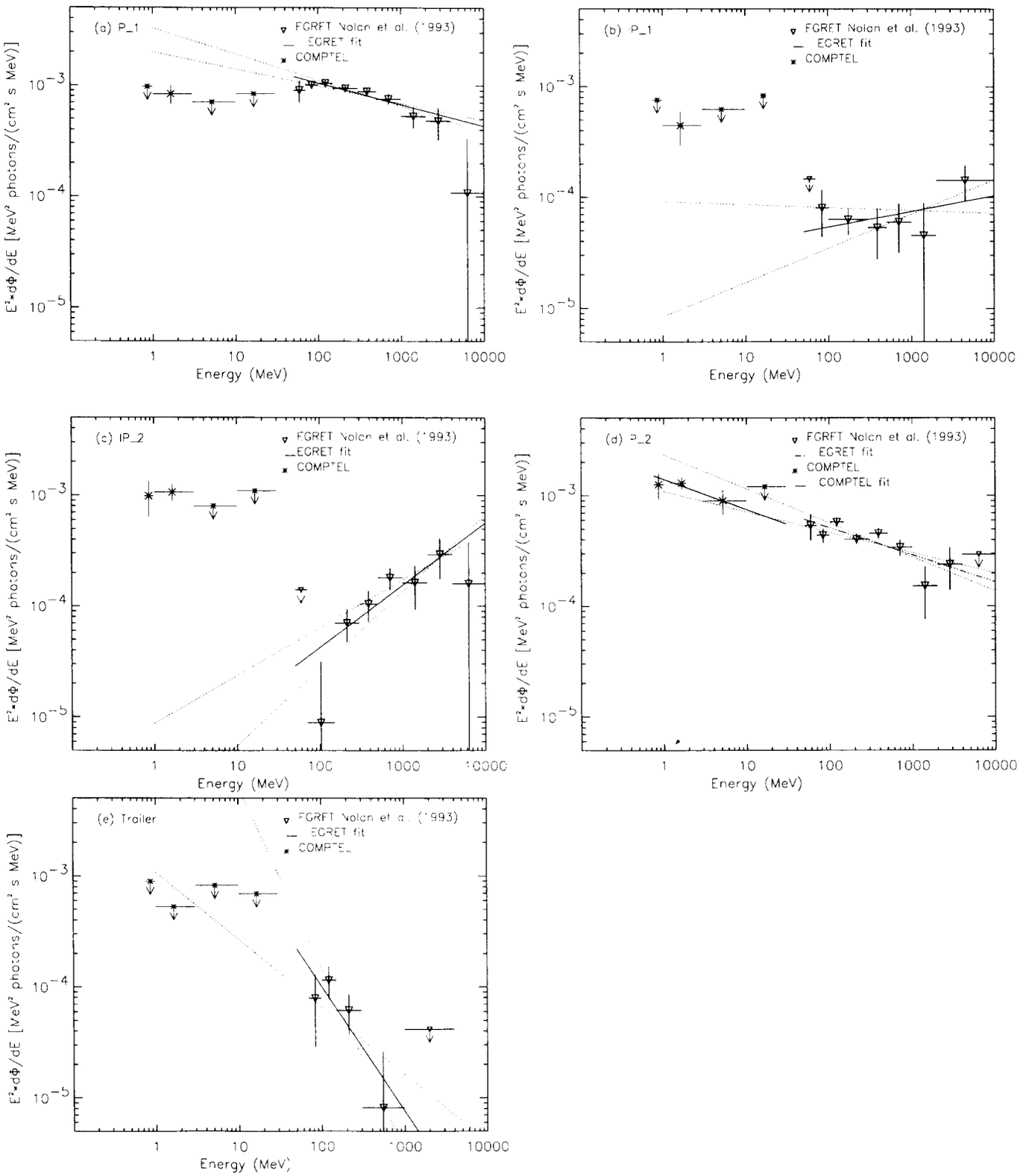

Fig. 7. Differential instantaneous phase-resolved spectra of the combined observations of the Crab pulsar multiplied by E^2, (a) first pulse, (b) interpulse 1, (c) interpulse 2, (d) second pulse and (e) trailer. The EGRET data and the EGRET power-law fits are also displayed. Dotted lines illustrate the 1σ uncertainty of the EGRET power-law fit parameter.

& Harding 1992). If the synchrotron emission from the downstream electron flow is fitted to the X- and γ-ray spectra, the optical and near-infrared spectra of the nebula are predicted correctly, although a time variability is not predicted. However Arons *et al.* (1993) have shown in one-dimensional simulations that a transverse shock in a pure pair plasma creates a fully thermalized downstream medium, which is in contradiction to the measured γ-ray power-law spectrum requiring a power-law electron distribution. Therefore Arons *et al.* (1993, 1994) added to the upstream flow an additional ion component with a γ-factor $\gamma=10^6$, corresponding to the possible acceleration energy of protons in a polar-cap. The electron and positron distributions emerging the shock front follow power-laws and the ions are thermalized.

In this context a plausible origin of the time variable γ-ray emission is a time dependant shock structure as suggested by Arons (1994, private communication). Time variability of the shock structure was found by Hoshino *et al.* (1992) in their simulations. Increases in the magnetic field strength may be associated with the intrinsic time dependence of the shock structure, which can cause time variable synchrotron losses of the γ-ray energy emitting particles.

5.2. Pulsed Emission

The pulsed emission of the Crab may be explained by the polar-cap or the outer-gap model. The current outer-gap model does not have a good geometrical prescription of the gap in the azimuthal direction, which largely controls the pulse profile. Currently a test on the "global" shape of the spectrum is more critical on the model than the normalization (Ho 1994, private communication). A characteristic of the outer-gap model is the predicted dip in the spectrum around 10 MeV in the transition region between the synchrotron and the inverse Compton scattering component.

A knee of the emitted power above 400 keV is obvious from Figure 5. There is further a dip in the phase-averaged emission above 4 MeV (two high energy COMPTEL and low energy EGRET data points), in agreement with the outer gap model predictions (Ho, 1989). However the significance of this dip in the data is weak due to the large uncertainties in the flux values at these energies. A detailed model fitting of the phase-averaged pulsed Crab spectrum over the full CGRO energy range using a consistent set of phase definitions and observation periods is in preparation (Ulmer *et al.* 1995).

The structure seen so far in the phase-averaged spectrum favours the outer-gap model, as the polar-cap model predicts a simple power-law between 1 MeV and several hundred MeV (Harding & Daugherty 1993). It should be noted that up to now simulations of the polar-cap model have been concentrated on the part of the spectrum above 10 MeV (Harding & Daugherty 1993; Chiang & Romani 1992). Above this energy the interaction of primary particles is most important, thus the inverse Compton process of low energy photons has not been taken into account. A future extension of calculations in the polar-cap model to lower energies, which includes the inverse Compton process, is therefore desirable.

Chiang and Romani (1992) pointed out that phase-resolved spectra may probe the physics of the pulsar magnetosphere emission. The present analysis constrains the shape of the phase-resolved spectra: a simple extrapolation of the EGRET best fit power-law into the COMPTEL energy range cannot describe the COMPTEL data, except for the second peak, where the COMPTEL data points lie within the 1σ uncertainty of the EGRET best fit power-law.

The phase-resolved spectra of the first and second peak (Fig. 7 a,d) are in agreement with the numbers obtained for the P_2/P_1 ratios in Table 4. A constant slope of the P_2 energy spectrum is observed, so that the decrease of the P_2/P_1 ratio with increasing energy directly reflects the flattening of the P_1 energy spectrum at higher energies.

Unfortunately, predictions for the phase-resolved spectra of the Crab pulsar are not available or not applicable to the interpretation of the COMPTEL data. Phase-resolved calculations within the polar-cap model are either restricted to energies above 10 MeV (Chiang & Romani 1992) or they are only calculated for small phase widths which are too narrow for our analysis (Harding & Daugherty 1993). Despite of this, in a comparison between calculations of the polar-cap model (Chiang & Romani 1992) and the EGRET measurements, Harding and Daugherty (1993) found that the *impact parameter* must be less than one. This dimensionless parameter is defined as the polar-cap radius expressed as fraction of the radius in the standard pulsar model of Goldreich and Julian (1969). The spectra calculated by Chiang and Romani (1992) for an impact parameter greater than one are much flatter than those observed. Presently, the outer-gap model of Ho (1989, 1993) lacks predictions for phase-resolved spectra. The current model gives the particle distribution in momentum space along a set of field lines pointing at the same tangent under simplified geometry (Ho 1993). A realistic calculation has to take into account the distribution of electrons along field lines pointing at different tangents. The radiation emitted from these field lines will be spread out over a range of angles, but also the electron distribution itself has a latitudinal and longitudinal component. Both will affect the pulse profile and thus the phase-resolved spectra. A comparison of our results with phase-resolved model spectra for a different set of parameters is highly desirable, as it may help to constrain the gap geometry and the electron distributions.

6. Summary

The COMPTEL experiment has shown its ability to provide valuable information for the discussion of theoretical

models of the Crab Pulsar and Nebula. Below 1 MeV the unpulsed flux is consistent with earlier measurements (e.g. Bartlett *et al.* 1993). There is evidence ($> 4\sigma$) for a time variability of the unpulsed emission on a time scale of 16 months. The phase-averaged spectrum of the pulsed emission is in agreement with the adjacent energy bands as measured by GRIS, OSSE and EGRET. There are indications for a dip in the power-per-decade spectrum for energies above 4 MeV. The phase-resolved analysis revealed that only the second peak can be described with a simple power-law from low MeV to GeV energies. For other phase intervals, a simple extrapolation of the EGRET best fit power-law cannot describe the COMPTEL data. At least one break in the spectra is required. The light curve resembles that seen by OSSE at hard X-ray energies. The pulsed count fraction of P_2/P_1 is consistent with the value reported by OSSE and differs from the EGRET measurements. The interpulse emission is proportionally more intense in the COMPTEL energy range than at higher energies as seen by EGRET.

The combination of the Crab observations analysed in the present work with follow-up observations will improve statistics and so enable us to make our statements more restrictive, especially regarding the phase-resolved analysis.

Acknowledgements. We thank the referee. J.L. Masnou, for his useful commments which helped to improve the content of this paper. R. Much acknowledges receipt of a research fellowship from the European Space Agency. The COMPTEL project is supported by the German government through DARA grant 50 QV 90968, by NASA under contract NASS-26645 and by the Netherlands Organisation for Scientific Research (NWO).

References

Agrinier B., et al., 1990, ApJ, 355, 645
Akerlof C.W., et al., 1990, Nucl. Phys. B, 14A, 237
Arons J., et al., 1993, in Proc. Los Alamos Workshop on Physics of Isolated Pulsars, ed. K. Van Riper, R.I. Epstein, C. Ho, (Cambridge: Cambridge Univ. Press), 336
Arons J., Tavani M., 1994, ApJS, 90, 797
Arzoumanian Z., Nice D., Taylor J. H., 1992, GRO/radio timing data base, Princeton University
Bartlett L.M., et al., 1993, in "The Second Compton Symposium", eds. C.E. Fichtel, N. Gehrels & J.P. Norris, (AIP: New York) Vol. 304
Bloemen H., et al., 1994, Proc. INTEGRAL Workshop, ApJS, 92, 419
de Boer H., et al., 1992, Proc. 4^{th} International Workshop on "Data Analysis in Astronomy", Erice, Italy (Plenum Press)
Buccheri R., et. al., 1993, Adv. Space Res., Vol. 13, No. 12, p. (12) 727
Busetta M., et al., 1992, Proc. 4^{th} International Workshop on "Data Analysis in Astronomy", Erice, Italy (Plenum Press)
Carramiñana A., et al., 1995, A&A, in press
Chiang J., Romani R., 1992, ApJ, 400, 629
Cheng K.S., Ho C., Ruderman M., 1986a, ApJ, 300, 500
Cheng K.S., Ho C., Ruderman M., 1986b, ApJ, 300, 522
Clear J., et al., 1987, A&A, 174, 85
Connors A., et al., 1992, Proc. of 4^{th} International Worshop on 'Data Analysis in Astronomy', Erice, Italy (Plenum Press)
Daugherty J.K., Harding A.K., 1982, ApJ, 252, 337
Diehl R., et al., 1992, Proc. of 4^{th} International Worshop on 'Data Analysis in Astronomy', Erice, Italy (Plenum Press)
Goldreich P., Julian W.H., 1969, ApJ, 336, 869
Graser U., Schönfelder V., 1982, ApJ, 263, 677
Harding A., 1981, ApJ, 245, 267
Harding A.K., Daugherty J.K., 1993, in Proc. Los Alamos Workshop on Physics of Isolated Pulsars, ed. K. Van Riper, R.I. Epstein, C. Ho, (Cambridge: Cambridge Univ. Press), 281
Harnden F.R., Seward F.D., 1984, ApJ, 283, 279
Hillier R.R., et al., 1970, ApJ, 162, L177
Ho C., 1989, ApJ, 342, 396
Ho C., 1993, in Proc. Los Alamos Workshop on Physics of Isolated Pulsars, ed. K. Van Riper, R.I. Epstein, & C. Ho, (Cambridge: Cambridge Univ. Press), 271
Hoshino M., et al., 1992, ApJ, 390, 454
De Jager O.C., Harding A.K., 1992, ApJ, 396, 161
De Jager O.C., et al., 1994, in "The Second Compton Symposium", eds. C.E. Fichtel, N. Gehrels & J.P. Norris, (AIP: New York) Vol. 304, p72
Jung G.V., 1989, ApJ, 338, 972
Kamae T., Sekimoto Y., 1994, Proc. of Yamagato Pulsar Workshop
Kanbach G., et al., 1990, in The EGRET Science Symposium, ed. C. Fichtel et al., (NASA Conf. Pub. 3071), 101
Kennel C.F., Coroniti F.V., 1984, ApJ, 283, 710
Lampton M., et al., 1976, ApJ, 208, 177
Masnou J.L., et al., 1994, A&A, 290, 503
Natalucci L., et al., 1991, Adv. Space Res., Vol. 11, No.8, (8)79
Nolan P.L., et al., 1993, ApJ, 409, 697
Parlier B., et al., 1973, Nature Phys. Sci., 242, 117
Ruderman M.A., Sutherland P.G., 1975, ApJ, 196, 51
Schönfelder V., et al., 1993, ApJS, 86, 629
Strong A.W., et al., 1992, Proc. 4^{th} International Workshop on "Data Analysis in Astronomy", Erice, Italy (Plenum Press)
Strong A.W., et al., 1993, A&AS, 97, 133
Sturmer S.J., Dermer C. D., 1994, ApJ, 420, L79
Ulmer M.P., et al., 1994, ApJ, 432, 228
Ulmer M.P., et al., 1995, ApJ, submitted
Vacanti G., et al., 1991, ApJ, 377, 467
Weekes T.C., et al., 1989, ApJ, 342, 379
White R., et al., 1985, ApJ, 299, L23
Worrall D.M., 1990, Proc. 23rd ESLAB SYMP., ESA SP-296, 719
Worrall D.M., Wilkes B.J., 1990, ApJ, 360, 396

This article was processed by the author using Springer-Verlag LaTeX A&A style file *L-AA* version 3.

A&A manuscript no.
(will be inserted by hand later)

Your thesaurus codes are:
01(13.07.2)

ASTRONOMY
AND
ASTROPHYSICS
15.3.1995

The detection of an unidentified variable gamma-ray source by COMPTEL

O.R.Williams[4], R. Much[4], K. Bennett[4], H. Bloemen[2], W. Collmar[1], W. Hermsen[2], G.G. Lichti[1], M. McConnell[3], J. Ryan[3], V. Schönfelder[1], H. Steinle[1], and C. Winkler[4]

[1] Max-Planck Institut für Extraterrestrische Physik, P.O. Box 1603, D-85740 Garching, Germany
[2] SRON-Utrecht, Sorbonnelaan 2, 3584 CA Utrecht, The Netherlands
[3] University of New Hampshire, Institute for the Studies of Earth, Oceans and Space, Durham NH 03824, USA
[4] Astrophysics Division, ESTEC, 2200 AG Noordwijk, The Netherlands

March 15, 1995

Abstract.

We report the detection of an unidentified, high galactic latitude, γ-ray source (GRO J1753+57) by the COMPTEL instrument onboard the Compton Gamma-ray Observatory. The source was clearly detected during observations in November 1992 and had a flux in the 1-3 MeV band of approximately half that of the Crab. All other observations of this region by COMPTEL only yield upper limits, or marginal detections, showing that this source is highly variable on a timescale of weeks. Possible counterparts are discussed.

Key words: Gamma rays: observations

1. Introduction

The COMPTEL instrument onboard the Compton Gamma Ray Observatory (CGRO) is the first imaging γ-ray telescope to be flown on a satellite, which covers the energy range between $\sim$ 0.75 MeV and 30 MeV (Schönfelder et al. 1993). Prior to the launch of COMPTEL, only a handful of observations at these wavelengths had been made, thus the first priority of COMPTEL was to perform an all sky survey. However, such a survey gives only a 'snapshot' of the sky, and some early results from the repeat viewing by COMPTEL showed evidence for source variability e.g. the bright quasars 3C 273 and 3C 279 (Williams et al. 1994). The large $\sim$ 1 steradian field of view of COMPTEL implies that subsequent serendipitous detections of sources which were in a 'low state' during previous observations are to be expected.

In this paper we present the detection of such a variable source during observations in November 1992. We also present the upper limits obtained from other observations of this source.

Send offprint requests to: O.R.Williams

2. Observations and Data Analysis Methods

2.1. Observations

COMPTEL (Schönfelder et al. 1993) has an energy resolution which ranges from $\sim$10% at 1 MeV to $\sim$5% at 30 MeV. In a typical 14 day viewing period (VP) the 3σ point source sensitivity is 1.6×10^{-4} photons s^{-1} cm^{-2} in the 1-30 MeV range, so it is able to detect sources which are about 20 times weaker than the Crab. Different sources within its circular $\sim$ 1 steradian field of view can be resolved if they are separated by more than $\sim 3^{\circ}$. The positional determination accuracy depends on the source strength, but is better than 1° for a source as strong as the Crab.

In this paper we report on data from the first 28 months of COMPTEL's operation in which the region around (l,b)=(85.5°,30.5°) was in the field of view (See Table 1).

Table 1. CGRO observations used in this paper

VP	Start	End	Pointing	
	dd-mm-yy	dd-mm-yy	l(°)	b(°)
2	30-01-91	08-06-91	73.3	2.6
9.5	12-09-91	19-09-91	59.7	40.3
201	17-11-92	24-11-92	79.8	36.4
202	24-11-92	01-12-92	102.8	35.6
203	01-12-92	22-12-92	111.0	21.7
212	09-03-93	23-03-93	84.3	11.4

2.2. Data Analysis Methods

The analysis of COMPTEL data is not straightforward since simple event projection onto the sky is not possible. Instead a hypothesised γ-ray sky, or single point source, is convolved with a 3-dimensional energy-dependent point response function (Diehl et al. 1992) into an 3-dimensional dataspace and then compared with measured events in that dataspace.

A maximum-likelihood method has been used to search for γ-ray sources within the 3-dimensional COMPTEL data-

space (de Boer et al. 1992). At each position within the field of view the likelihood $L(H^o)$ is calculated for the null hypothesis H^o that the observed data arises only from a background distribution; the background being estimated from the measured data using a filtering technique (Bloemen et al. 1994). Similarly the maximum-likelihood $L(H^1)$ is calculated for the hypothesis that the data is explained by the same background distribution plus a point-like source. In a classical interpretation, the quantity -2lnλ (where $\lambda = L(H^1)/L(H^o)$) is distributed as χ^2_q, with q being the number of free parameters that are added to the null hypothesis. The values of -2lnλ over the field of view can be displayed and are referred to as maximum-likelihood ratio maps (MLMs).

With this maximum-likelihood method flux values with their associated statistical errors may be determined in the selected energy ranges. Since the point-spread function is slightly energy dependent, an input energy spectrum has to be assumed in order to obtain flux values. Throughout this analysis an E^{-2} spectrum has been used: any uncertainty in the flux measurements due to this will be $\lesssim 5\%$.

3. Results

3.1. Detection and Variability

Within the routine analysis of COMPTEL data, MLMs are created for four standard energy intervals: 0.75-1, 1-3, 3-10, 10-30 MeV. Figure 1 shows the 1-3 MeV MLMs of the two observations in November 1992 (VP 201 and 202). There is clear evidence (5σ for 3 degrees of freedom) of a source at (l,b)=(85.5°,30.5°) in VP 201, hereafter designated GRO J1753+57. Even if we take into account that we made 24 trials (4 energy intervals, 6 observations) then the probability of random events simulating the signal is still $<2\times10^{-5}$. Moreover, in the map of VP 202 we find further evidence for GRO J1753+57. In a single trial, valid given the significant detection in VP 201, we find a signal of 3.6σ significance at the position of GRO J1753+57 in VP 202.

Table 2 gives the fluxes in the four standard energy bands determined at the position (l,b)=(85.5°,30.5°) during all observations. Apart from the clear detections in VP 201 and 202 the other observations yield only upper limits or marginal detections.

Table 2. Fluxes determined at (l,b)=(85.5°, 30.5°), and the angle between this (l,b) and COMPTEL's pointing direction

Obs	Offaxis	Flux (10^{-6} photons cm^{-2}s^{-1})			
	(°)	0.75-1	1-3	3-10	10-30 (MeV)
2	30.1	<139	<140	<135	<24
9.5	23.2	<179	<138	<72	<28
201	17.8	<247	489±91	<122	<22
202	15.7	186±99	288±94	<121	<49
203	30.5	<70	<88	56±27	<28
212	18.9	<94	110±51	<80	<20

The 1-3 MeV 'lightcurve' of GRO J1753+57 shown in Fig. 2 demonstrates significant variability. In particular, the flux must decline by at least a factor of 2.3 (at 2σ significance) between VP 201, when a high flux was detected, and VP 203, when only an upper limit was measured.

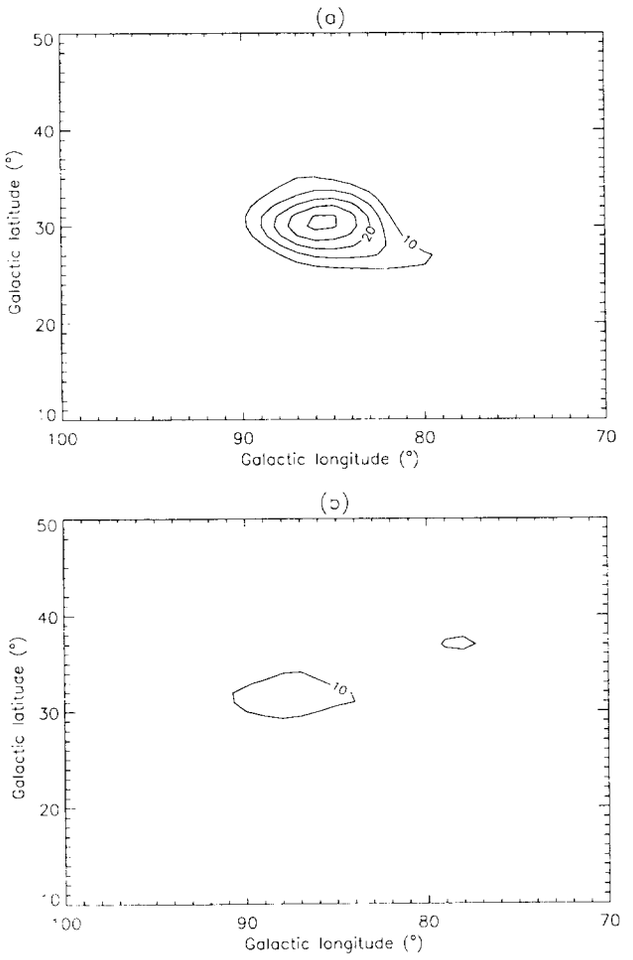

Fig. 1. MLMs of the 1-3 MeV range for VPs (a) 201 and (b) 202

3.2. Energy Spectra

By adding together the two observations in November 1992 and adopting narrower energy bins we can better define the spectrum. Table 3 shows the energy bands used and the fluxes obtained. Figure 3 shows the energy-density spectrum derived from these numbers. For the purposes of comparison Fig. 3 also shows a broken power-law with slopes of $\alpha = -1.8$ below 2 MeV and $\alpha = -2.4$ above 2 MeV: such a shape is known to fit the 3C 273 spectrum obtained in June 1991 (Williams et al. 1994).

We note that a single power-law fit to the photon spectrum is only acceptable at the 90% level ($\chi^2/\nu = 6.1/3$). Moreover a broken power-law fit (with the break energy fixed at 2 MeV) yields $\chi^2/\nu = 0.9/2$, an improvement which is 94% significant according to the F test. Finally, we note that an extension of the single power-law slope ($\alpha = -2.3 \pm .2$) to higher energies would imply a detectable flux in the co-aligned EGRET instrument, while smoothed EGRET intensity maps for VP 201 and 202 show no feature at this location.

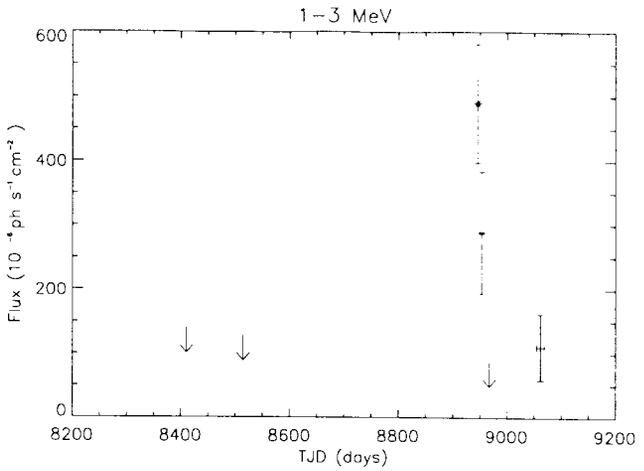

Fig. 2. 1-3 MeV 'Lightcurve' of GRO J1753+57

Therefore the data suggest a spectrum similar to the MeV emission of objects such as 3C 273 (Lichti et al. 1994) and GRO J01516-609 (Bloemen et al. 1994b), with either a peak in the energy-density spectrum, or at least a break of slope, within the COMPTEL energy range.

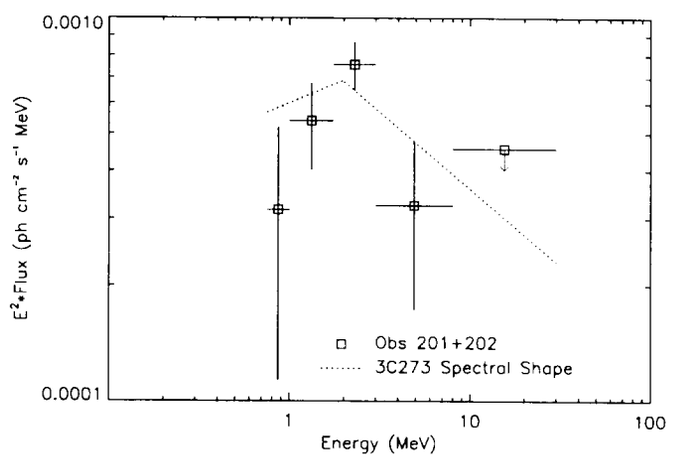

Fig. 3. Luminosity spectrum during VP 201+202 compared with the spectral shape of 3C 273 (Williams et al. 1994)

Table 3. Fluxes at (l,b)=(85.5°,30.5°) for VP 201 and 202

Energy (MeV)	Flux (10^{-6} photons cm^{-2}s^{-1})
0.75-1.00	105±67
1.00-1.75	228±59
1.75-3.00	180±40
3.00-8.00	67±31
8.00-30.0	<41

3.3. Possible Counterparts

We have searched the X-ray catalogues within the EXOSAT database (Reynolds & Parmar 1993), together with the Hewitt & Burbidge (1993) and Veron-Cetty & Veron (1993) AGN catalogues, for sources within a 5° cone centred on (l,b)=(85.5°,30.5°). In addition, we have checked the SIMBAD catalogues (Egret, Wenger & Dubois 1991) for sources designated as radio or X-ray emitters in a region of 8°×8°centred on the same position as before. Discounting clusters we found 12 sources in total: SAO 030826, 1ES 1817+537, H 1811+540, 4C 56.27, 1H 1801+579, NGC 6418, SAO 03041, IPC 172600+59, HD 160934, 4C 61.34, NGC 6393, NGC 6454. Finally, the two closest objects in the EGRET source catalogue are the QSO 1739+522 and an unidentifed source GRO J1837+59, but both lie too far away to be considered good candidates.

In Table 4 we give the locations and some information on the objects discussed in this section. If an object is included by virtue of its X-ray emission, then the X-ray catalogue in which the object is listed is given. In Fig. 4 we show the uncertainties in the location of GRO J1753+57, overlaid with the locations of possible counterparts: we see that only NGC 6454, NGC 6418, and 1H 1801+579 lie within the 3σ contour.

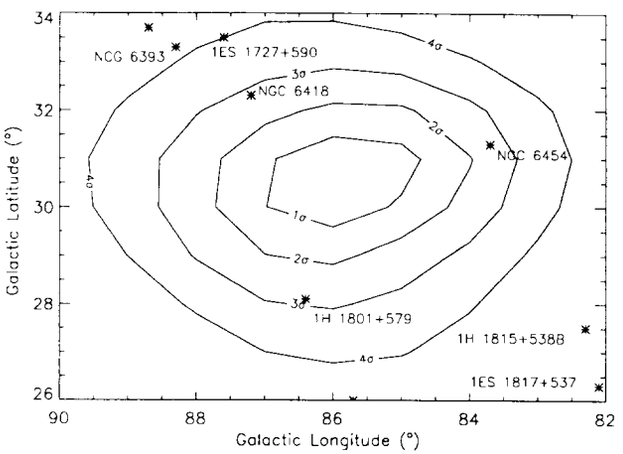

Fig. 4. Contour plot showing the uncertainty in the location of GRO J1753+57. Overlaid are the positions of potential counterparts

4. Discussion

It is currently not possible to identify counterparts of GRO J1753+57 at other wavelengths and so a discussion of possible physical models is inappropriate.

We cannot exclude a galactic origin for this source. However of the 34 sources clearly detected at high galactic latitudes (l >10°) by EGRET (Fichtel et al. 1994) 25 are blazar type AGN with compact, flat-spectrum, radio cores while the remainder are unidentified except for the LMC. It is therefore natural to look for counterparts amongst blazar type AGN, particularly since they can vary on timescales of a few days e.g. 3C 279 (Kniffen et al. 1993). Moreover the COMPTEL source GRO J01516-609 (Bloemen et al. 1994b), which is thought to be emission from one or more blazar type objects, has a COMPTEL spectrum similar to the source discussed in this paper. However, the closest known blazar type objects, the

Table 4. Details of X-ray , γ-ray and radio selected objects near the location of GRO J1753+57

Name	Alternative name	X-ray cat.	Class	l (°)	b (°)	Ang. dist. from GRO J1753+57
1H 1815+538.A	SAO 030826	A3	RS CVn star	82.0	27.0	4.6°
1ES 1817+537		IPC	Unclassified	82.2	26.3	4.9°
1H 1815+538.B	H 1811+540	A3	Seyfert I	82.3	27.2	3.9°
IPC 182319+56	4C 56.27	IPC	BL-Lac/Quasar	85.7	26.1	4.3°
1H 1801+579		A3	Star(?)	86.4	28.1	2.3°
1H 1741+586	NGC 6418	A3	Seyfert I	87.2	32.3	2.4°
1ES 1727+590	SAO 030416	IPC	Star	87.6	33.6	3.6°
IPC 172600+59		IPC	unclassified	88.7	33.8	4.3°
1ES 1737+612	HD 160934	IPC	Star	90.2	32.3	4.4°
IPC 174222+61	4C 61.34	IPC	QSO radio loud	90.8	31.7	4.7°
NGC 6393			Seyfert II	88.3	33.3	3.8°
NGC 6454			Radio Bright Galaxy	83.7	31.3	1.8°
QSO 1739+522			EGRET QSO	79.5	32.0	5.3°
GRO J1837+59			Uniden. EGRET src.	88.	25.	6.0°

BL-Lac 4C 56.27 and the radio loud QSO 4C 61.34, lie well outside the 4σ location contours shown in Fig. 4.

The radio emitting elliptical galaxy NGC 6454 is one of three X-ray selected objects within the 3σ uncertainty in the location of GRO J1753+57. Interestingly, it has a redshift of $z = 0.032$ and a compact flat-spectrum radio core with a "jet" like extension (Brindle & Fomalont 1978). However, it has a significantly lower luminosity in the radio, optical, and X-ray (Fabbiano et al. 1982) than the extragalactic sources previously detected by COMPTEL.

The other X-ray selected objects within the 3σ uncertainty contour of the source location are 1H 1801+579 and the Seyfert galaxy NGC 6418 (Remillard et al. 1993). Prior to the launch of the CGRO Seyfert galaxies were expected to be strong emitters in the soft γ-ray region and detections had been claimed for NGC 4151 and MCG 8-11-11 (Perotti et al. 1981). However, COMPTEL has yet to detect emission from a Seyfert galaxy (Maisack et al. 1994) and OSSE measurements show that Seyfert galaxies typically have thermal spectra above 50 keV. It is of course possible that emission on the level of that recorded from NGC 4151 and MCG 8-11-11 occurs only as a transient phenomena, in which case this variable source could indeed be a Seyfert galaxy. We note that the observed spectrum is compatible with those claimed earlier for NGC 4151 and MCG 8-11-11.

5. Conclusion

We have detected a new bright variable γ-ray source GRO J1753+57 in the low energy γ-ray range. During a period of three weeks it declines from an intensity approximately half that of the Crab to below the COMPTEL detection threshold. The non discovery of such a bright source during the all-sky survey demonstrates the transient nature of the emission from at least some sources of soft γ-rays .

Acknowledgements.

The COMPTEL project is supported by the Deutsche Agentur für Raumfahrtangelenheiten (DARA) under the grant 50 QV 90968, by NASA under contract NAS5-26645, and by the Netherlands Organisation for Scientific Research NWO. We thank K.Dennerl for searching the SIMBAD database.

References

Bloemen H., Hermsen W., Swanenburg B.N., et al., 1994, ApJS, 92, 419.

Bloemen H., Bennett K., Blom J.J.,et al. 1994b, A&A, in press.

de Boer H., Bennett K., Bloemen H., et al., 1992, in: Data Analysis in Astronomy IV, ed. V. Di Gesu et al., Plenum Press, New York, p. 241.

Brindle, A.H., Fomalont, E.B., 1978, AJ, 83, 704.

Diehl R., Aarts H., Bennett K., et al., 1992, in: Data Analysis in Astronomy IV, ed. V. Di Gesu et al., Plenum Press, New York.

Egret D., Wenger M., Dubois P., 1991, in: Databases and Online Data in Astronomy, ed. M.A. Albrecht & D. Egret, Kluwer Academic Publishers, p.79.

Fabbiano G., Feigelson E., Zamorani G., 1982, ApJ, 256, 397.

Fichtel C.E., Bertsch D.L., Chiang J, et al., 1994, ApJS, 94, 551.

Hewitt A., Burbidge G., 1993, ApJS, 87, 451.

Kniffen D.A., Bertsch D.L., Fichtel C.E., et al., 1993, ApJ., 411, 133.

Lichti G.G., Balonek T., Courvoisier T.J.-L., et al., 1994, A&A, in press.

Maisack M., Collmar W., Barr P., et al., 1994, A&A, in press.

Perotti F., Della Ventura A., Villa G., et al., 1981, Nature, 292, 133.

Remillard R.A., Bradt H.V.D., Brissenden R.J., et al. 1993, AJ, 105, 2079.

Reynolds A.P., Parmar A., 1993, in: Astronomical Data Analysis and Software Systems II, ed. R.J. Hanish, R.J.V. Brissenden, J. Barnes, ASP Conf. Series, Vol 52, p.70.

Schönfelder V., Aarts H., Bennett K., et al., 1993, ApJS, 86, 657.

Veron-Cetty M.-P., Veron P., 1984, ESO Sci Rept., No.1, 1.

Williams, O.R., Bennett K., Bloemen, J.B.G., et al., 1994, A&A, in press.

A&A manuscript no.
(will be inserted by hand later)

Your thesaurus codes are:
13.07.1

ASTRONOMY
AND
ASTROPHYSICS
14.3.1995

Gravitational lensing origin for a possible gamma–ray burst repeater?

L.O. Hanlon[4], W. Hermsen[2], R.M. Kippen[3], S.M. Matz[5], K.S. O'Flaherty[4], R.D. Preece[6], J. Ryan[3], V. Schönfelder[1], O.R. Williams[4], and C. Winkler[4]

[1] Max-Planck-Institut für Extraterrestrische Physik, Postfach 1603, D-85740, Garching, Germany
[2] SRON-Utrecht, Sorbonnelaan 2, 3584 CA Utrecht, The Netherlands
[3] University of New Hampshire, Institute for the Studies of Earth, Oceans and Space, Durham NH 03824, USA
[4] Astrophysics Division, Space Science Department of ESA/ESTEC, NL-2200 AG Noordwijk, The Netherlands
[5] Department of Physics and Astronomy, Northwestern University, Evanston, IL 60208, USA
[6] Dept. of Physics, University of Alabama in Huntsville, AL 35899, USA

March 14, 1995

Abstract. One observational consequence of a cosmological distribution of γ–ray bursts is that some recurrent bursts, due to gravitational lensing, should be seen during the lifetime of the *Compton* Gamma–Ray Observatory. These would be identifiable by their spatial coincidence and by their identical time profiles and spectra.

The COMPTEL experiment, onboard the *Compton* Gamma–Ray Observatory, has imaged two γ–ray bursts (GRB 930704 and GRB 940301) with coincident locations, separated in time by eight months. We report here on the spectral and temporal analysis of these two events in order to establish whether they are gravitationally lensed images of the same burst. We conclude that although the envelopes of the time profiles are similar, they are sufficiently different on short timescales to rule out the standard lensing hypothesis. Furthermore, spectral dissimilarities between the pair mitigate against the possibility that the differences in time profiles could have arisen through microlensing. Since lensing is ruled out, the remaining possibilities are an accidental coincidence of unrelated bursts or a true repeating burst source. The latter would severely constrain cosmological burst models.

Key words: Gamma–rays: bursts

1. Introduction

Since the discovery by the Burst and Transient Source Experiment (BATSE) onboard the *Compton* Gamma–Ray Observatory (CGRO), of the isotropic distribution of even the faintest γ–ray bursts (Meegan et al. 1992), cosmological theories of their origin have become more favoured. Recently, a 'stretching' in the profiles of dim bursts relative to bright ones has been reported (Norris et al. 1994). This is consistent with bursts at BATSE's peak-flux completeness limit being at cosmological distances corresponding to $z \sim 1$. If γ–ray burst (GRB) sources are a cosmological population, they should be gravitationally lensed about as frequently as quasars, with differences in light travel time of between a few months and a few years (Paczyński 1986). Since current γ–ray detectors cannot resolve the small separations between the images, lensed GRBs could be identified by their apparent spatial coincidence and by their identical (within a scale factor) spectra and time histories.

The COMPTEL instrument, onboard CGRO, has imaged two events (GRB 930704 and GRB 940301) with coincident locations, separated in time by eight months, out of a dataset of 17 bursts (Kippen et al. 1995). The probability of this spatial coincidence being due to chance is 3%, based on COMPTEL observations alone. Interplanetary Network localisations reduce this probability to 1.5%. Although studies based on the first BATSE catalogue showed some evidence for a significant fraction of repeating GRBs (Wang & Lingenfelter 1993; Quashnock & Lamb 1993), further analysis utilising a larger BATSE sample constrains the fraction of repeating bursts to be less than 10% (Hartmann et al. 1994). We investigate the possibility that the pair of events imaged by COMPTEL are not repeating episodes from a single source, but rather are double images caused by gravitational lensing of the GRB source by a foreground galaxy. A search for lensed pairs in a sample of 611 BATSE bursts produced no definite candidates (Nemiroff et al. 1994). The closest pair of events identified in that study were separated by 3.7°. The Pois-

Send offprint requests to: L.O. Hanlon

son probability of this spatial coincidence being due to chance is $\sim 36\%$, when systematic uncertainties ($\sim 4°$) are included. The GRBs under consideration here were not included in the investigation of Nemiroff et al.

Although all four instruments on-board CGRO are capable of recording γ–ray burst time profiles and spectra, we deal here primarily with the analysis of COMPTEL, OSSE and BATSE data. The COMPTEL instrument has two separate modes in which GRB data can be acquired (Schönfelder et al. 1993; Winkler et al. 1986). In 'burst' mode two of COMPTEL's NaI detectors acquire moderate time resolution spectra in two overlapping energy regions, 0.1–1.5 MeV and 0.6–10.6 MeV (122 and 128 energy channels respectively). The time resolution is 1 s for 6 s after receipt of the burst trigger from BATSE, then 6 s for a further 900 s, after which the detector returns to background mode, integrating for 100 s. Low range data only are considered here, due to the poor statistics of these GRBs in the high range. The 'telescope' mode utilises the full instrument to derive source locations and spectra in the range 0.75–30 MeV.

The BATSE data type DISCSC, from the Large Area Detectors (Fishman et al. 1994) provides timing information with 64 ms resolution and four-channel discriminator data from 25 keV up to 10 MeV.

The OSSE experiment accumulates high time resolution (16 ms) GRB profiles above 100 keV from its large area NaI shields (Share et al. 1986).

2. Time Profile Comparison

In order to test the lensing hypothesis the time profiles of the two events were first compared using the COMPTEL low range 'burst' module data, over the energy range 0.1–1.5 MeV (Fig. 1).

Qualitatively, the time profiles are similar, in that they exhibit a fast rise, with an exponential decay to background. This is a relatively common GRB profile envelope, dubbed 'FRED' (Fast Rise Exponential Decay) and 7% of BATSE bursts comprise this subclass (Bhat et al. 1994).

The time profiles of the two events, in the energy range 0.1–1.5 MeV, were background subtracted using an average background count rate after the burst had decayed. Variable scaling factors and time shifts (between T_{trig} and $T_{trig}+42$ s, where T_{trig} is the BATSE trigger time) were applied to GRB 930704, and each iteration was compared with the 'template' profile of GRB 940301 until a minimum in χ^2 was obtained. The χ^2 test for two binned data sets (Press et al. 1992) was used to determine the compatibility of the data sets. This comparison method is similar to those used in previous searches for lensed GRB candidates (Nemiroff et al. 1994; Wambsganss 1993). The minimum χ^2 of 5.7 for 4 degrees of freedom (where both bursts are above their respective background levels) was found for a time shift (δt_{min}) of 12 s relative to the BATSE trigger and a scaling factor (f_{min}) of 8.0 and implies that

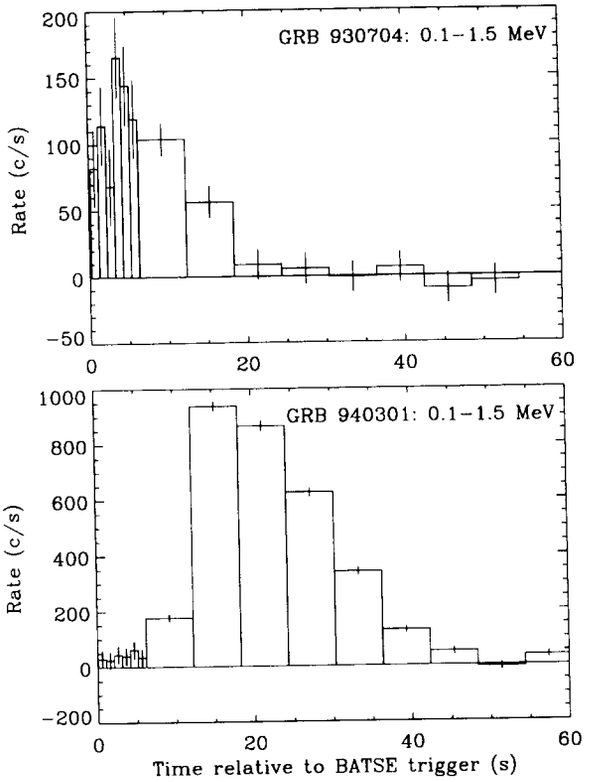

Fig. 1. COMPTEL background subtracted time histories for GRB 930704 (upper panel) and GRB 940301 (lower panel) between 0.1 and 1.5 MeV

there was no significant difference between the bursts on this timescale (Fig. 2).

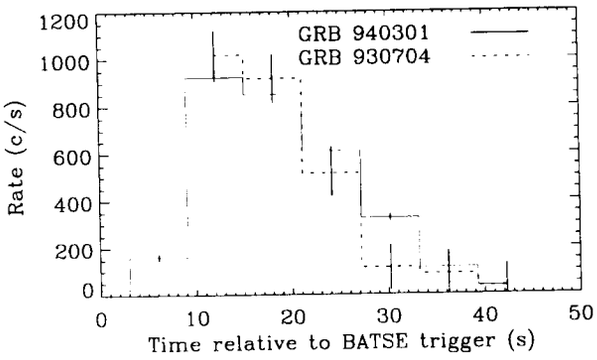

Fig. 2. COMPTEL scaled and time shifted profile of GRB 930704 is shown with the 'template' profile of GRB 940301

This result is not surprising, given that both profiles have the typical 'FRED' shape and duration. Furthermore, the averaged time profiles of GRBs tend to be non-symmetric, having a shorter rise time than decay time (Mitrofanov et al. 1994). For the gravitational lensing hypothesis to be strongly tested, the time profiles must be

identical (to within Poisson errors) on even the shortest timescales (Paczyński 1986). Therefore, the same χ^2 comparison technique was applied to the OSSE data (16 ms time resolution) for the two events, yielding a minimum χ^2/ν of 4307/2269. Thus, on these shorter timescales, the two events are significantly different. The OSSE scaled and shifted profiles are shown in Fig. 3.

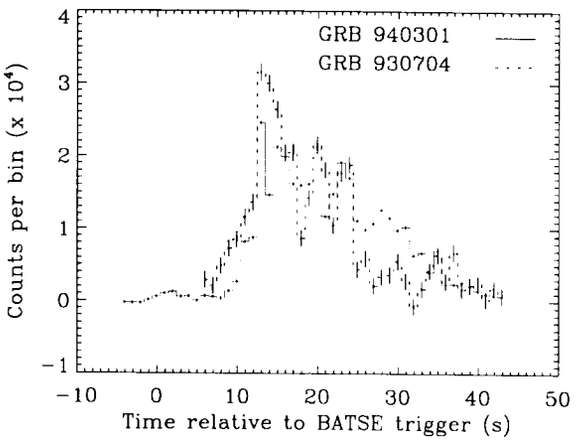

Fig. 3. OSSE scaled and time shifted profile of GRB 930704, shown with the 'template' profile of GRB 940301. Data have been rebinned into 1 s bins for clarity. δt_{min} = 6 s; f_{min} = 6.3 (see text for definitions)

3. Spectral Comparison

The spectra of the two events are expected to be identical (within a magnification factor) if they are caused by lensing of a point source. Time integrated spectra from the COMPTEL low range 'burst' module were fitted using a standard forward folding technique in the energy range 0.3–1.5 MeV, using a power law photon model (see Hanlon et al. 1994 for details). The time intervals for the deconvolution were T_{trig}+12 to T_{trig}+48 s for GRB 940301 and T_{trig} to T_{trig}+36 s for GRB 930704, which were chosen to match the minimum χ^2 interval obtained from the COMPTEL time profile comparison.

A best fit power law index of -2.43±0.07 (χ^2/ν = 43/43) was obtained for GRB 940301, while a value of -2.25±0.88 (χ^2/ν = 1.1/2) was obtained for GRB 930704. These results indicate that the spectra for both events are compatible (Fig. 4). However, the COMPTEL uncertainties for GRB 930704 are substantial due to the low statistics.

Most GRBs undergo spectral evolution, usually a softening, over their duration (Norris et al. 1986). Therefore, not only must the time averaged spectra of the two events concur, but also the evolution of the spectra within the bursts.

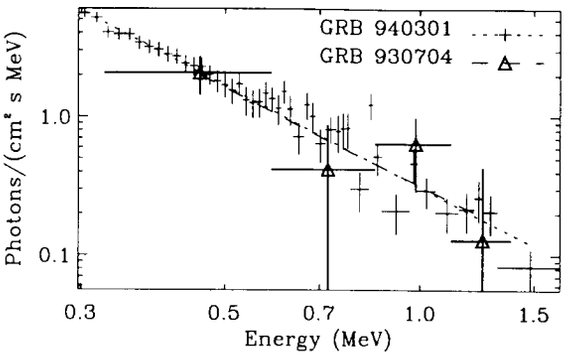

Fig. 4. Deconvolved COMPTEL photon spectra over the time interval T_{trig}+12 to T_{trig}+48 s for GRB 940301 and T_{trig} to T_{trig}+36 s for GRB 930704. The lines represent the best photon models for the spectra (dotted and dashed for 940301 and 930704 respectively). GRB 930704 has been scaled by a normalisation factor

Hardness ratios, in the energy bands 25–100 keV and 100–300 keV, were computed using the BATSE DISCLA, DISCSC and PREB summed data types, with 1 s resolution. The data were background subtracted using a 4^{th} order polynomial model derived from time intervals before and after the burst. In order to quantify differences in the relative hardnesses the χ^2 comparison method was applied as before. A minimum χ^2 of 96 for 34 degrees of freedom was obtained for δt_{min} = 2.048 s and f_{min} = 1.754. The scaling factor (f) is a free parameter which is not strictly allowed in the lensing hypothesis since both events should have compatible relative hardnesses if they have been lensed. However, by including this parameter in the χ^2 minimisation procedure, the discrepancy in the spectral behaviour of the two bursts is clearly demonstrated (Fig. 5). If the procedure is repeated allowing only a time shift as the free parameter, a minimum χ^2/ν = 447/20 is obtained, for δt_{min} = 15.36 s. The differences in spectral behaviour of these two bursts provide ineluctable evidence against a lensing origin.

4. Discussion

The fact that the brighter event followed the weaker one does not in itself rule out a gravitational lensing scenario; a spherical lens with a finite core radius can occasionally produce this configuration of lensed images (Blaes & Webster 1992). However, the analysis of the temporal data for GRBs 930704 and 940301 shows conclusively that even though the two events are globally similar in shape and duration, there are significant differences between them on short timescales. The differences in time profiles would appear to rule out a gravitational lensing origin for the two events.

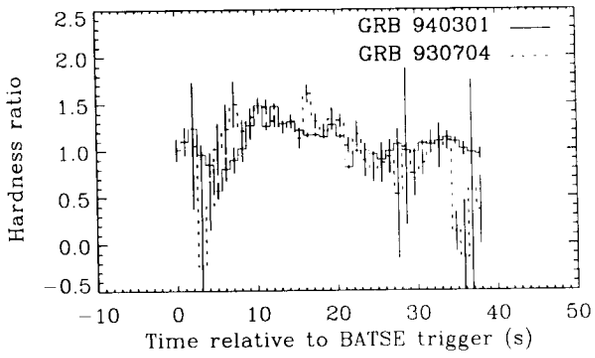

Fig. 5. Hardness ratios for GRB 930704 and GRB 940301 from BATSE data. The GRB 930704 data are shown scaled and time shifted by amounts which minimise the differences relative to GRB 940301. Even then, the spectral behaviour is clearly different

A possible lensing scenario which may give rise to such differences could involve microlensing by individual compact objects in the lensing galaxy. For example, if the radiation is highly beamed, with the beaming angle as small as the bending angle due to microlensing, then the observed temporal variability in the two images may differ (Paczyński 1987; Babul et al. 1987). In order for the source to appear isotropic to the macrolens the condition $\gamma_l \leq 10^8 \times M_6{}^{-1/2}$ must hold, where γ_l is the bulk Lorentz factor and M_6 is the lens mass in units of 10^6 $M_\odot$ (Blaes & Webster 1992). The time delay of 8 months between the appearance of the two GRBs implies a lensing mass of approximately 5×10^{11} $M_\odot$ (Mao 1992). Therefore, $\gamma_l \leq 1.4 \times 10^5$ is required in order for the source to appear isotropic to the lensing galaxy.

A lower limit on γ_l for GRB 940301 (the most constraining of the pair) has been estimated from COMPTEL data. The shortest variability observed in the telescope data was 150–200 ms at an energy of 6.2 MeV. Assuming a source distance of 1 Gpc and a spectral slope of -2.7, we derive $\gamma_l \geq 11.4$ (Baring 1994). More stringent lower limits estimated for previous GRBs e.g. $\gamma_l \geq 10^3$ for GRB 930131 (Sommer et al. 1994) still do not violate the isotropy inequality. Furthermore, the cosmological relativistic fireball models require $10^2 \leq \gamma_l \leq 10^5$ (Mészáros & Rees 1993). It is therefore highly unlikely that γ_l exceeds the value demanded for isotropy of the source with respect to the lensing galaxy. The possibility of microlensing by stellar type objects can thus be excluded, since the source is isotropic to the lensing galaxy and therefore to micro-objects within it.

The different spectral hardnesses of the pair further mitigate against a lensing origin, since light bending is an achromatic process. The physical properties of matter along the two light paths would have to be different in order to give rise to such spectral differences.

5. Conclusions

We have shown that a gravitational lensing origin for these two spatially coincident GRBs may be ruled out. The probability of the spatial coincidence being random is $\sim 1.5\%$, from COMPTEL and IPN measurements. We therefore cannot discount the hypothesis that the positional overlap is merely a chance occurrence. The third possibility is that the two events are separate burst episodes from a single source. If that is the case, then cosmological models must be revised since many invoke singular cataclysmic events such as neutron star/neutron star or neutron star/black hole coalescence (Narayan et al. 1992) or failed Type 1b supernovae (Woosley 1993) as the origin of the γ-ray emission.

Acknowledgements. LOH wishes to acknowledge the Education Programme of the European Community for providing a fellowship, ESA for providing facilities to carry out this work, and B. McBreen and C. Kouveliotou for helpful discussions. K.S. O'F acknowledges an ESA fellowship. The COMPTEL project is supported by the German goverment through DARA grant 50 QB 9096 8, by NASA under contract NASA-26645 and by the Netherlands Organisation for Scientific Research (NWO).

References

Babul, A., Paczyński, B., Spergel, D. 1987, ApJ, 316, L49
Baring, M. 1994, ApJS, 90, 899
Bhat, P., Fishman, G., Meegan, C. et al. 1994, ApJ, 426, 604
Blaes, O., Webster, R. 1992, ApJ, 391, L63
Fishman, G., Meegan, C., Wilson, R. et al. 1994, ApJS, 92, 229
Hanlon, L., Bennett, K., Collmar, W. et al. 1994, A&A, 285, 161
Hartmann, D., Blumenthal, G., Hurley, K. et al. 1994, 127–131, American Institute of Physics, New York
Kippen, R., Bennett, K., Connors, A. et al. 1995, A&A, 293, L5
Mao, S. 1992, ApJ, 389, L41
Meegan, C., Fishman, G., Wilson, R. et al. 1992, Nat, 355, 143
Mészáros, P., Rees, M. 1993, ApJ, 405, 278
Mitrofanov, I., Chernenko, A., Pozanenko, A. et al. 1994, 187–191, American Institute of Physics, New York
Narayan, R., Paczyński, B., Piran, T. 1992, ApJ, 395, L83
Nemiroff, R., Wickramasinghe, W., Norris, J. et al. 1994, ApJ, 432, 478
Norris, J., Nemiroff, R., Scargle, J. et al. 1994, ApJ, 424, 540
Norris, J., Share, G., Messina, D. et al. 1986, ApJ, 301, 213
Paczyński, B. 1986, ApJ, 308, L43
Paczyński, B. 1987, ApJ, 317, L51
Press, W., Teukolsky, S., Vetterling, W., Flannery, B. 1992, Numerical Recipes, Chapt. 14, Cambridge University Press
Quashnock, J., Lamb, D. 1993, MNRAS, 265, L59
Schönfelder, V., Aarts, H., Bennett, K. et al. 1993, ApJS, 86, 657
Share, G., Johnson, W., Kinzer, R. et al. 1986, Adv. Space Res., 5(4), 15
Sommer, M., Bertsch, D., Dingus, B. et al. 1994, ApJ, 422, L63
Wambsganss, J. 1993, ApJ, 406, 29

Wang, V., Lingenfelter, R. 1993, ApJ, 416, L13
Winkler, C., Schönfelder, V., Diehl, R. et al. 1986, Adv. Space Res., 6, 113
Woosley, S. 1993, ApJ, 405, 273

This article was processed by the author using Springer-Verlag LaTeX A&A style file *L-AA* version 3.

A&A manuscript no.
(will be inserted by hand later)

Your thesaurus codes are:
06(13.07.1; 13.07.2; 03.19.2; 02.18.5)

ASTRONOMY
AND
ASTROPHYSICS
14.3.1995

COMPTEL observations of the strong gamma–ray burst GRB 940217

C. Winkler[4], R.M. Kippen[3], K. Bennett[4], W. Collmar[1], L.O. Hanlon[4], W. Hermsen[2], K.S. O'Flaherty[4], J. Ryan[3], V. Schönfelder[1], H. Steinle[1], and O.R. Williams[4]

[1] Max-Planck-Institut für extraterrestrische Physik, D-85740 Garching, Germany
[2] SRON-Utrecht, Sorbonnelaan 2, NL-3584 CA Utrecht, The Netherlands
[3] University of New Hampshire, Institute for the Studies of Earth, Oceans and Space, Durham NH 02384, USA
[4] Space Science Department of ESA, Astrophysics Division, ESTEC, NL-2200 AG Noordwijk, The Netherlands

Received: 20 February 1995; accepted: 13 March 1995

Abstract. The imaging MeV gamma-ray telescope COMPTEL on board the *Compton* Gamma-Ray Observatory has observed a very strong ($S[> 0.3$ MeV$] = 2.03 \times 10^{-4}$ erg cm^{-2}), complex, and long lasting (162 s) gamma-ray burst on February 17, 1994 (GRB 940217). The burst consists of several peaks. Temporal fluctuations occur on timescales as short as 100 ms. Hard–to–soft spectral evolution has been observed during the burst emission and also within individual peaks. The photon spectra obtained within the peaks can be modelled by single power law spectra and by broken power laws with break energies at around 1 MeV. The best-fit power law slopes vary between 1.1 and 3.5 throughout the event. The spectra are consistent within COMPTEL's different observing modes and also agree very well with contemporaneous EGRET and BATSE measurements. No significant line emission is detected in any of the recorded spectra. Precise location ($[\alpha_{2000}, \delta_{2000}] = [29.5°, 3.8°]$, with a 3σ error radius of about 1°) has been obtained through direct COMPTEL MeV imaging in combination with timing analysis by the Interplanetary Network. Four hours after the event, the position derived by COMPTEL was distributed to a network of multi-wavelength observers. No detection of a fading or quiescent counterpart has so far been reported at any wavelength. During a 20 minute time interval starting $\sim$ 90 minutes after the burst event, the EGRET instrument on board the *Compton* Gamma-Ray Observatory reported "post-burst" emission at high energies (up to GeV). COMPTEL does not detect any significant "post-burst" emission at low energies (0.3 – 30 MeV), and our upper limits are marginally consistent with the EGRET detections. Using high energy spectral and temporal information, distance limits to GRB 940217 between 145 AU and 11.7 kpc have been derived assuming homogenous and isotropic emission. If GRB 940217 is at cosmological distances (e.g. at 1 Gpc) the lower limit on the relativistic bulk Lorentz beam factor is >18. This implies that our observed breaks at around 1 MeV are either too low in energy to be produced by γ–γ interaction (via e^+e^- – pair creation), or GRB 940217 is closer than 1 Gpc.

Key words: gamma-ray bursts: observations – non-thermal processes

Send offprint requests to: C. Winkler (e-mail [internet]: cwinkler@estsa2.estec.esa.nl)

1. Introduction

The imaging gamma-ray telescope COMPTEL, one of four instruments on board the *Compton* Gamma Ray Observatory (CGRO), has been operating since April 5, 1991. The gamma-ray burst of February 17, 1994 (GRB 940217) was the strongest and one of the longest lasting events observed in the field of view (FOV) of COMPTEL during the first 3 years of operations, therefore rendering it a prime candidate for detailed spectral and imaging investigations. COMPTEL observations of similar events (including e.g. GRB 910425, GRB 910503, GRB 910601, GRB 910814, GRB 930131) have been reported earlier by Winkler et al. (1992a, 1992b, 1992c), Varendorff et al. (1992), Collmar et al. (1993), Connors et al. (1993), Ryan et al. (1994), Hanlon et al. (1994), and Kippen et al. (1994b).

2. Instrument and operating modes

COMPTEL operates in two different modes during the observation of gamma-ray bursts. In its "double scatter mode" (or telescope mode) photons are Compton scattered from one of the upper liquid scintillator detectors over $\sim$ 1.5 m down to one of the lower NaI crystals. This

mode allows for the re-construction of the source direction ("direct imaging") within a FOV of $\sim$ 1 sr, provides spectra over 0.75 – 30 MeV and time histories with 125 μs resolution. In its "single detector mode" two of the lower NaI detectors simultaneously accumulate spectra in two energy ranges 0.1 – 1.5 MeV (122 channels) and 0.2 – 10 MeV (128 channels), respectively. However, reliable detector response information (see Section 3.2.2) is only available for energies E > 0.3 MeV (low range) and E > 0.6 MeV (high range). The sequence of accumulated burst spectra in those detectors is initiated by receipt of a BATSE trigger signal. In the default mode, prior to the trigger, background spectra (100 s integration time each) are recorded until this sequence is interrupted by the receipt of the BATSE trigger signal and subsequently 6 spectra (each of 1 s integration time), followed by 133 spectra (each of 6 s integration time) are accumulated. Finally the background mode is re-entered awaiting the next BATSE trigger. Spectral resolution for both modes is < 9.5% (E > 0.5 MeV). A detailed description of the COMPTEL instrument can be found in Schönfelder et al. (1993).

3. Observational data and results

On February 17, 1994 (Truncated Julian Day (TJD) = 9400) at UT = 82962 s, an outburst of celestial high energy gamma radiation was reported by BATSE (trigger # 2831) which triggered the "single detector mode" of COMPTEL, while a total of $\sim$ 740 photons were obtained in the "double scatter mode".

3.1. Time histories

Deadtime corrected lightcurves from the event are shown for different energy ranges in Figures 1 and 2. The burst emission commences $\sim$ 6 seconds after the onset (at UT = 82962 s) and largely consists of 6 well separated peaks (Table 1) with a total duration of 162 s.

Table 1. GRB 940217: Time intervals used for spectral analysis (see Figures 1 and 2). T_{start} = start of the integration time of "single detector mode" spectra.

Peak #	T_{start} (s)	Duration (s)
Full burst	82962.12	162
1	82968.21	30
2	83022.44	6
3	83046.56	18
4	83070.66	12
5	83088.75	18
6	83112.87	12

We note already from Figures 1 and 2, that the relative peak amplitudes vary with energy indicating different spectral shapes of individual peaks (see also Section 3.2 and Figures 3 and 6).

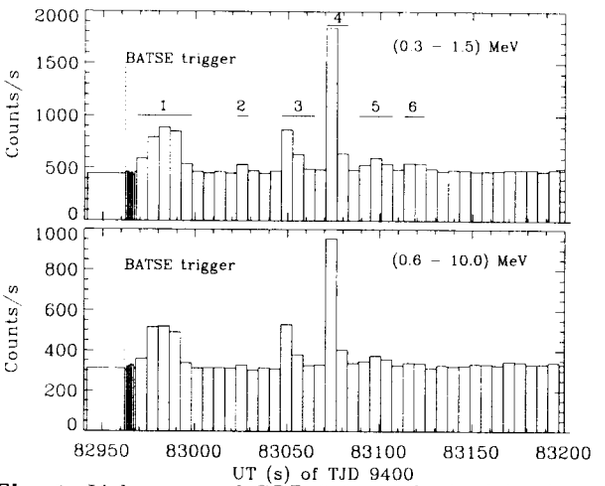

Fig. 1. Lightcurves of GRB 940217 obtained in the "single detector mode", upper panel = low energy range, lower panel = high energy range. Time intervals containing peaks #1 – #6 used for spectral deconvolution of both ranges are indicated.

The "double scatter mode" (telescope) lightcurve was examined by binning the events on smaller and smaller time scales until significant variation was no longer visible. The fastest temporal variations have a full width of $\sim$ 100 ms. Several of these occurred throughout the burst, the shortest is within analysis peak #4 (Figure 2, inset).

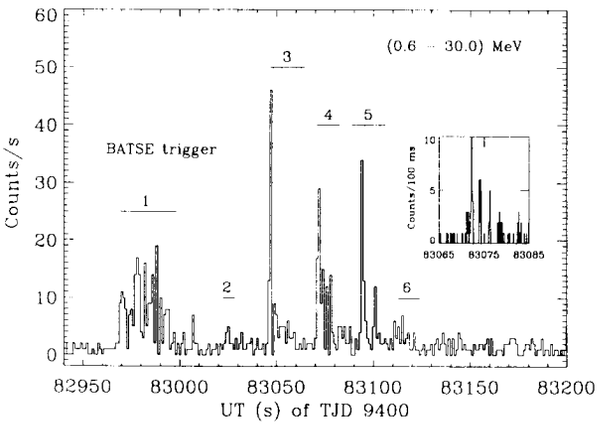

Fig. 2. Lightcurve of GRB 940217 obtained in the "double scatter mode" with 1 s binning. Time intervals containing peaks #1 – #6 used for spectral deconvolution are indicated and are identical to the ones shown in Figure 1. The inset displays fast temporal variations with 100 ms binning during peak #4.

3.2. Spectral analysis

3.2.1. Spectral evolution

Hardness ratios (Figure 3) were computed for all spectra obtained in the "single detector mode" and within all the 6 lightcurve peaks (Figure 1). We used background subtracted counts from two energy ranges (0.1 – 0.3 MeV and 0.3 – 1.5 MeV) of the low range detector. In general, hardness ratios from this detector have better statistics compared to those derived using data from the high and low range detectors. The background was determined by fitting a 2nd order polynomial to the 0.1 – 1.5 MeV data (see Section 3.2.2). Each data point in Figure 3 represents a 6 s integration time. We note an overall trend of hard–to–soft evolution both within individual peaks and from peak to peak. A least squares fit to the data shows significant deviation (12.4σ) from a line of zero slope, although this fit is formally only a poor model of the hardness evolution ($\chi^2 = 227$ for 14 d.o.f.). Apart from the global trend we note that peak #1 becomes harder after 6 s followed by a softening. Peak #4, the last 12 s of peak #5 and peak #6 also show softening. Peak #2 is relatively soft before the burst apparently gets harder again at the onset of peak #3. Besides the general hard–to–soft evolution described above, the data alternatively suggest a "2–fold" evolution consisting of peaks #1 and #2, and peaks #3 to #6 (Figure 3). Again, the slope of each subset deviates significantly from a flat hardness ratio.

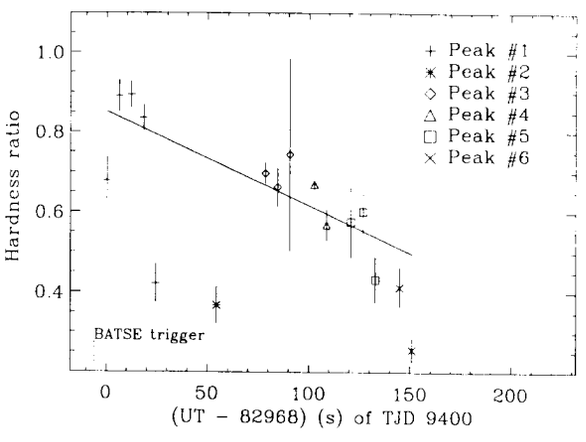

Fig. 3. Hardness ratios for GRB 940217. The hardness ratio was calculated using background subtracted counts from low range data ([0.3 – 1.5 MeV]/[0.1 – 0.3 MeV]) in "single detector mode". Statistical error bars shown are 1σ.

3.2.2. Photon spectra

Single detector mode The count spectra obtained in "single detector mode" were processed as follows: a background was subtracted from all deadtime corrected and energy calibrated spectra. This background is estimated from the observed background spectrum (100 s integration time) obtained prior to the burst onset multiplied by a time dependant scaling function to account for the (mainly orbital) long–term temporal variation of the background during the burst emission. The scaling function was determined by fitting the background, excluding the period of burst emission (162 s duration), with a polynomial: the long term trend in the background (outside the time interval shown in Figure 1) is energy dependant and has been fitted with a 1st order polynomial for the low range data, and with a 2nd order polynomial for the high range data. The spectral fitting of these background subtracted data was performed using a standard forward folding technique of convolving a trial photon spectrum with the detector response matrix, covering both ranges, into a count spectrum. The two energy ranges were treated individually. The location of the burst (see Section 3.3.1) in the instrument coordinate system (zenith = 10.35°, azimuth = 308.93°) was used in calculating the effective detector area. The convolved trial photon spectrum was then compared with the observed spectrum in count space and a minimum χ^2 was iteratively determined for the best–fit photon spectrum. A single power law spectrum was used as the trial input. In this model, the photon flux is given by $a \times E^{-\alpha}$ with normalization a [photons/(cm^2 s MeV)] at 1 MeV, energy E [MeV], and slope α.

In the case that the hypothesis of a single power law could not be accepted (on >5% level) because of too large χ^2 values, the fit was repeated using a broken power law model with 4 parameters a (as above), break energy E_{break} [MeV], and power law slopes α_{low} and α_{high} below and above E_{break}, respectively.

The errors on the best–fit parameters were estimated using the prescription given by Lampton et al. (1976): following their Table 1, 90% confidence intervals (1.6σ) for the parameters fitted simultaneously were obtained by using the parameter space between χ^2_{min} and $\chi^2_{min} + \Delta$, where $\Delta = 4.61$ for 2–parameter fits (single power law) and $\Delta = 7.78$ for 4–parameter fits (broken power law).

Prior to spectral fitting, the background subtracted spectra were rebinned in order to ensure that each bin contains a sufficient number of counts to validate the application of χ^2 statistics. Starting from the high energy end of the spectral range the energy bins were combined until the number of counts in the new bin exceeds the background by 3σ. In general this results in an energy dependant bin size, with the bin size increasing with energy.

χ^2 tests were applied in the energy ranges 0.3 – 1.5 MeV for low range spectra, and 0.6 – 10 MeV for high range spectra. The energy ranges are determined by the boundaries of the available energy response matrix information (see Section 2).

Detailed results obtained by fitting trial photon spectra to both ranges are shown in Table 2 (single power laws) and Table 3 (broken power laws). The majority of

the fitted photon spectra can indeed be described by single power laws with slopes ranging from $\alpha = 1.78^{+0.52}_{-0.38}$ (peak #5) to $\alpha = 3.52^{+0.88}_{-1.00}$ (peak #2). A least squares fit to the data (power law slopes vs. time) of Table 2 shows a 2.6σ deviation from a flat line.

The high range data for peaks #1, #4 and for the full burst duration fail to accept the hypothesis of a single power law model and require a broken power law fit with break energies at around 1 MeV. High range data for peaks #2 and #6 could not be used for spectral deconvolution, because due to the low flux (cf. Figure 1), the 3σ-rebinning (see above) resulted in a small number of energy bins which was insufficient for spectral fitting. As an example the photon spectrum for the full burst event (162 s, Tables 2 and 3) is shown in Figure 4.

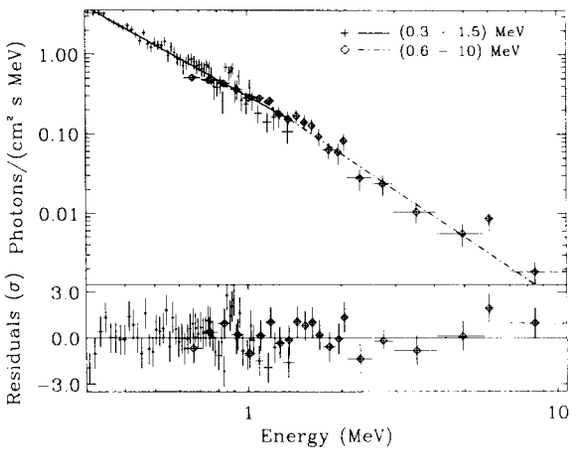

Fig. 4. Photon spectrum of GRB 940217 (full burst, 162 s duration) obtained in "single detector mode". The solid line is the best-fit single power law to low range 0.3 – 1.5 MeV data with normalization $a = 0.30 \pm 0.02$ photons/(cm^2 s MeV), and slope $\alpha = 2.15 \pm 0.12$. The dashed line is the best-fit broken power law to high range 0.6 – 10.0 MeV data with $a = 0.32^{+0.09}_{-0.06}$ photons/(cm^2 s MeV), and slopes $\alpha_{low} = 1.25^{+0.85}_{-1.20}$ and $\alpha_{high} = 2.63^{+0.77}_{-0.35}$ below and above the break energy $E_{break} = 1.07^{+0.75}_{-0.35}$ MeV, respectively.

Double scatter mode The telescope 0.75 – 30 MeV data were fitted within the same intervals (peaks) as used for the "single detector mode" data (Table 1, Figures 1 and 2). Here, a single power law photon spectrum with slope $\alpha = 2.0$ was simulated at the proper burst position (see Section 3.3.1) in order to determine the instrument energy response function. The response is found to be insensitive to the exact shape of the trial spectrum (provided the energy bins are larger than the instrument resolution). By selecting only those events which originate close to the derived source direction, photons which are incompletely absorbed in the lower detector are eliminated (Schönfelder et al. 1993). This selection results in three main effects: (i) the energy response matrix is (nearly) diagonal which reduces matrix inversion to scalar multiplication; (ii) the background is significantly reduced; (iii) the detection efficiency is reduced. This simulated energy response matrix is used to calculate the burst photon flux from the observed (deadtime corrected) count spectrum.

The standard COMPTEL event selection criteria applied include those for pulse shape, time–of–flight and energy (see Schönfelder et al. 1993 for a detailed description), as well as the additional constraint to select only those events within 10° of the derived burst location.

Model testing is performed by forward folding spectral models and comparing the model counts with the background (measured 15 orbits or $\sim$ 84000 s later) and with the observed data in count space. The Cash statistic (Cash 1976) is used to estimate model parameters and their uncertainties. This statistic cannot be used to directly derive a "goodness of fit" value, therefore random bootstrap simulation is applied. In each simulation, the best–fit model counts are randomized (poisson–distributed) and the Cash statistic is evaluated between the randomized spectrum and the best–fit model. For many such random samples this forms a distribution of Cash statistics which are due only to random deviations of the model. By examining where the Cash statistic of the observed data with the best–fit model falls in this distribution, we can determine if the data are consistent with the model ("goodness of fit").

The parameter of interest is the fraction of random samples with Cash statistics greater than that of the observed data. This is just the probability (Π) of observing a Cash statistic greater than that of the real data based only on random fluctuations of the model. This is equivalent to the probability of observing $\chi^2 > \chi^2_{min}$ implying that we can reject models with (1 – Π) confidence, but in general we expect $\Pi \sim 0.5$ which corresponds to $\chi^2/\nu = 1$.

We tested single power law, optically thin thermal bremsstrahlung (OTTB) and thermal synchrotron models. Single power laws are acceptable for all phases of the burst, and no broken power laws are required in the 0.75 – 30 MeV energy range. OTTB models can be rejected for the full burst, and for peaks #5 and #6. Synchrotron models can be rejected for the full burst and for peaks #4, #5 and #6.

Spectral fitting results using telescope ("double scatter mode") data are shown in Table 4. Errors on fit parameters are 90% confidence (1.6σ). Uncertainties in deadtime estimates lead to systematic normalization errors of up to 50%. The telescope photon spectrum for GRB 940217 (full burst duration of 162 s) is shown in Figure 5. The errors shown in Figure 5 are derived during the fitting process and are statistical errors only.

Comparison of Table 4 with Tables 2 and 3 and comparison of Figure 5 with Figure 4, shows very good agreement between the independent data obtained in the two

Table 2. GRB 940217: Single power law photon spectra ("single detector mode").

Time interval (see Table 1)	Range MeV	normalization a photons/(cm^2 s MeV)	slope α	$\chi^2_{d.o.f.}$	d.o.f.	Notes
Full burst	0.3 – 1.5	0.30 ± 0.02	2.15 ± 0.12	68.2	54	
Full burst	0.6 – 10.0	–		–	–	(a)
Peak #1	0.3 – 1.5	0.63 ± 0.04	1.86 ± 0.11	74.3	62	
Peak #1	0.6 – 10.0	–		–	–	(a)
Peak #2	0.3 – 1.5	$0.07^{+0.07}_{-0.04}$	$3.52^{+0.88}_{-1.00}$	3.4	4	
Peak #2	0.6 – 10.0	–	–	–	–	(b)
Peak #3	0.3 – 1.5	$0.41^{+0.04}_{-0.55}$	2.07 ± 0.20	37.2	39	
Peak #3	0.6 – 10.0	0.37 ± 0.05	$2.29^{+0.26}_{-0.19}$	16.0	12	
Peak #4	0.3 – 1.5	1.51 ± 0.08	2.20 ± 0.08	86.3	70	
Peak #4	0.6 – 10.0	–		–	–	(a)
Peak #5	0.3 – 1.5	$0.18^{+0.04}_{-0.06}$	2.15 ± 0.48	11.8	14	
Peak #5	0.6 – 10.0	0.11 ± 0.05	$1.78^{+0.52}_{-0.38}$	6.9	4	
Peak #6	0.3 – 1.5	$0.07^{+0.05}_{-0.04}$	3.30 ± 0.70	7.1	8	
Peak #6	0.6 – 10.0	–	–	–	–	(b)

Note: Errors on fit parameters are 90% confidence intervals (1.6σ).
(a): see Table 3 for broken power law fit
(b): see text

Table 3. GRB 940217: Broken power law photon spectra ("single detector mode").

Time interval (see Table 1)	Range MeV	normalization a photons/(cm^2 s MeV)	slope α_{low}	slope α_{high}	E_{break} MeV	$\chi^2_{d.o.f.}$	d.o.f.
Full burst	0.6 – 10.0	$0.32^{+0.09}_{-0.06}$	$1.25^{+0.85}_{-1.20}$	$2.63^{+0.77}_{-0.35}$	$1.07^{+0.75}_{-0.35}$	16.2	18
Peak #1	0.6 – 10.0	$0.68^{+0.17}_{-0.17}$	$1.40^{+0.73}_{-1.20}$	$3.25^{+2.55}_{-0.55}$	$1.22^{+0.98}_{-0.37}$	13.6	15
Peak #4	0.6 – 10.0	$1.80^{+0.20}_{-0.40}$	$1.13^{+0.97}_{-1.10}$	$2.59^{+0.45}_{-0.19}$	$1.00^{+1.00}_{-0.24}$	29.3	30

Note: Errors on fit parameters are 90% confidence intervals (1.6σ).

Table 4. GRB 940217: Single power law photon spectra ("double scatter mode") obtained in the 0.75 – 30 MeV range.

Time interval (see Table 1)	normalization a photons/(cm^2 s MeV)	slope α	Π
Full burst	$0.38^{+0.03}_{-0.03}$	$2.61^{+0.11}_{-0.11}$	0.52
Peak #1	$0.93^{+0.11}_{-0.11}$	$3.02^{+0.22}_{-0.20}$	0.32
Peak #2	$0.12^{+0.08}_{-0.06}$	$3.03^{+1.56}_{-0.90}$	0.90
Peak #3	$0.60^{+0.11}_{-0.10}$	$2.68^{+0.28}_{-0.26}$	0.18
Peak #4	$2.31^{+0.44}_{-0.39}$	$2.63^{+0.27}_{-0.25}$	0.82
Peak #5	$0.27^{+0.06}_{-0.05}$	$2.44^{+0.31}_{-0.27}$	0.59
Peak #6	$0.13^{+0.06}_{-0.05}$	$3.45^{+1.21}_{-0.85}$	0.60

Note: Errors on fit parameters are 90% confidence intervals (1.6σ).
Note: Probability Π (column 5): see text.

COMPTEL operating modes. Note that the break observed in "single detector mode" (Figure 4) is just at the low energy boundary of the telescope spectrum shown in Figure 5. The best-fit power law slopes derived from all data in both operating modes are shown for comparison in Figure 6. The telescope data in Figure 6 strengthen our conclusion made above, that the spectral slopes of the individual peaks are significantly different. In addition, the overall trend of hard–to–soft evolution as indicated by the hardness ratios (Figure 3) can be confirmed.

Finally, we have investigated whether our data show a correlation between hardness and intensity. As independent variable ("intensity") we use for each of the individual peaks #1 to #6 background subtracted counts obtained in the "single detector mode" low range (0.3 – 1.5 MeV). The dependant variable ("hardness") is given by

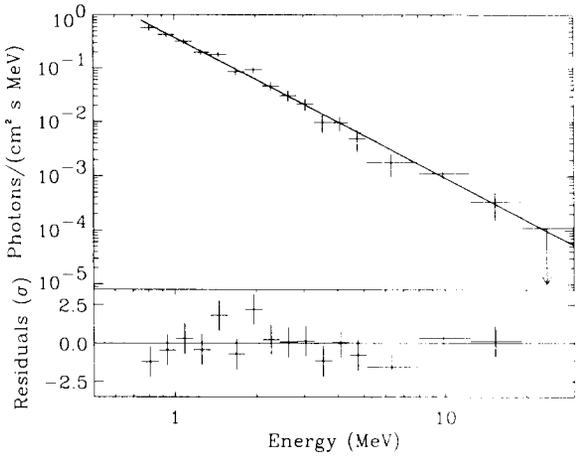

Fig. 5. Photon spectrum of GRB 940217 (full burst, 162 s duration) obtained in "double scatter mode". The best-fit single power law to the 0.75 – 30.0 MeV data is shown with $a = 0.38 \pm 0.03$ photons/(cm^2 s MeV) and slope $\alpha = 2.61 \pm 0.11$.

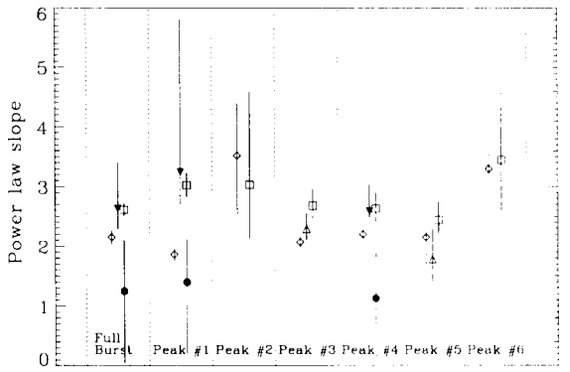

Fig. 6. GRB 940217: Best-fit power law slopes (α) for full burst and for peaks #1 to #6 obtained in "single detector mode" and "double scatter mode" (see Tables 2, 3, 4). *Single power law:* Diamonds: "single detector mode" low range 0.3 – 1.5 MeV. Open triangles: "single detector mode" high range 0.6 – 10.0 MeV. Squares: "double scatter mode" (telescope) 0.75 – 30 MeV. *Broken power law:* Filled circles: "single detector mode" high range 0.6 – 10.0 MeV below break energies at around 1 MeV. Filled triangles: "single detector mode" high range 0.6 – 10.0 MeV above break energies at around 1 MeV. Error bars are described by 90% confidence intervals.

the best-fit power law slopes per peak (fit energy range 0.3 – 1.5 MeV), as shown in Table 2 and Figure 6. A least squares fit to the data shows no significant deviation ($<1\sigma$) from a line of zero slope, indicating that the data are not correlated.

Comparison with other instruments In Figure 7 we have compiled the COMPTEL photon spectra (see above) together with the results from EGRET and BATSE data (Hurley et al. 1994c). The COMPTEL data cover the first 162 s of the burst event, while the EGRET and BATSE data were obtained during the first 180 s of the burst (Hurley et al. 1994c). The COMPTEL data do not show significant emission beyond 162 s, so that the results are comparable. The COMPTEL "single detector mode" data (see Figure 4) and "double scatter mode" data (see Figure 5) are shown again in Figure 7 as plain crosses and cover the energy range 0.3 – 30 MeV. The best-fit photon spectra to the COMPTEL data are given above (Figures 4 and 5). The best-fit photon spectrum obtained by the BATSE spectroscopy detectors (SD), covering the energy range 41 keV – 2.961 MeV (data = crosses with squares), is given by $dN/dE = (1.95 \pm 0.02) \times 10^{-2}$ (E/100 keV)$^{-1.215\pm0.02}$ $\times$ exp(−E/(838±63) keV) photons/(cm^2 s keV), and is shown as a solid line in Figure 7. The spectrum obtained by the EGRET total absorption shower counter (TASC) covers the energy range 0.9 – 200 MeV and the data (crosses with diamonds) are described by a single power law (dashed curve) with normalization $a = (3.6 \pm 0.26) \times 10^{-4}$ photons/(cm^2 s keV) at 1 MeV and slope $\alpha = 2.50 \pm 0.08$. The best-fit to the EGRET spark chamber data covers the energy range 30 – 4000 MeV and is given by a power law $(2.91 \pm 0.97) \times 10^{-7} \times$ (E/128 MeV)$^{-2.08\pm0.56}$ photons/(cm^2 s MeV) and is shown as dashed-dotted curve in Figure 7.

The overall consistency of the observations from three different instruments on board CGRO is remarkably good, in particular the consistency with COMPTEL and BATSE at energies below 1 MeV and consistency with COMPTEL and EGRET TASC. We note that the BATSE SD best-fit is somewhat low close to its sensitivity limit at ~3 MeV and that the EGRET spark chamber best-fit is not a high energy extrapolation of the TASC MeV data. This is also directly evident from the EGRET data points shown by Hurley et al. (1994c) and may indicate a possible turnover in the spectrum at around 50 MeV.

3.2.3. Fluence

GRB 940217 was the strongest burst observed so far by COMPTEL (see Hanlon et al. 1994 for a discussion on earlier events observed by COMPTEL): using the fit results for the full burst (162 s duration) from Tables 2 and 3 we obtain a fluence S(> 0.3 MeV) = 2.03 $\times 10^{-4}$ erg cm^{-2}.

3.2.4. Line emission

All individual "single detector mode" spectra accumulated during the burst emission (162 s) have been visually inspected in both ranges (0.3 – 1.5 MeV and 0.6 – 10.0 MeV, 32 spectra per range) and no significant emission or absorption feature had been detected. In addition, as described above, all spectra could be modelled using continuum spectra not requiring an additional spectral component (e.g. line feature). This negative result adds to the

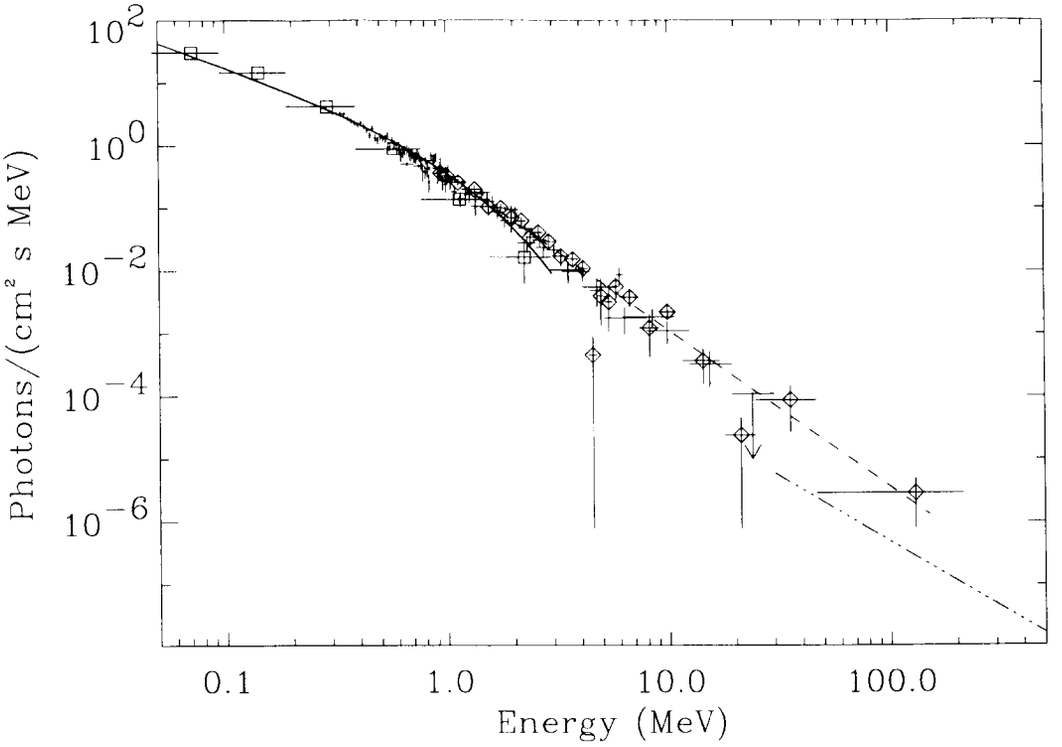

Fig. 7. Photon spectrum of GRB 940217 obtained with COMPTEL (data of both modes = plain crosses), BATSE (data = crosses with squares, best-fit = solid line), EGRET TASC (data = crosses with diamonds, best-fit = dashed line), and EGRET spark chamber (best-fit = dashed-dotted line). The BATSE and EGRET results are taken from Hurley et al. (1994c). See text for details.

earlier results that none of the COMPTEL gamma-ray bursts analysed so far (Winkler et al. 1992b, Hanlon et al. 1994 and references therein) have revealed any significant line feature in the data.

3.3. Spatial analysis

3.3.1. Location and counterparts

Imaging events observed in the "double scatter mode" are analysed in a three-dimensional data space defined by the two co-ordinates of the Compton scatter direction and the Compton scatter angle which are defined – via the Compton formula – by the electron rest mass energy and the energy deposits in the upper and lower detector arrays, respectively (Schönfelder et al. 1993). Using maximum likelihood analysis (de Boer et al. 1992) this data space is searched for the presence of a point source. This procedure reveals both the significance of the source and its position on the sky.

For GRB 940217, a total of 743 "double scatter mode" events (source and background) were selected from the full burst time interval (Table 1) with standard event selection filters for time-of-flight, pulse shape discrimination, energy deposits in both detector arrays and Compton scatter angle (Schönfelder et al. 1993). These events were binned into the three-dimensional data space with bin size of 1° for scatter direction and 2° for Compton scatter angle. A three-dimensional source model was generated by simulating a source power law (E^{-2}) spectrum, and a background model was generated by sampling events from orbit conditions similar to those during the burst observations. These correspond to events from a time interval taken 15 orbits ($\sim$ 1 day) after the event. After 15 orbits the spacecraft is again located at the same position above the earth surface (same suborbital points), so that the orbital radiation environment is nearly identical. Source and background scale factors were allowed to vary independently in order to fit the observed distribution of events as the maximum likelihood ratio was computed for each position on the sky around the most likely position. The parameters of interest from the resulting COMPTEL sky map of maximum likelihood ratios are: peak value = 18.8σ, peak position: (α_{2000}, δ_{2000}) = (30.1°, 3.1°), and (l,b) = (154.49°, - 55.49°). The COMPTEL location of this burst was communicated via the Rapid Response Network (Kippen et al. 1993, 1994a) $4^h\ 15^{min}$ after receipt of the BATSE trigger to initiate a world wide search for optical and radio counterpart emission. Radio observations began as soon as 5^h after the burst emission. So far no positive detections of quiescent

or fading counterparts have been reported (McNamara et al. 1995).

An *improved* burst location can be obtained by using the COMPTEL data together with results from the IPN (Interplanetary Network) triangulation arc (Hurley et al. 1994b). The annulus passes through the COMPTEL 1.8σ confidence contour, and the COMPTEL derived position (above) is only 0.9° away from the IPN annulus at its closest approach. A combined COMPTEL/IPN localization has been calculated by evaluating the COMPTEL maximum likelihood ratios at several points along the IPN annulus. Bicubic interpolation was used due to the coarse COMPTEL binning (~ degree). The most likely COMPTEL/IPN position is where the COMPTEL maximum likelihood ratio is highest along the arc. The confidence contours (1σ, 2σ, 3σ) have been determined from those values in the maximum likelihood map where the value of the maximum likelihood ratio (362.2) has dropped by 1, 4 and 9. The width of the IPN annulus is negligible compared to the intrinsic spatial resolution of COMPTEL. The parameters of interest from the resulting COMPTEL/IPN sky map of maximum likelihood ratios are: peak position: $(\alpha_{2000}, \delta_{2000}) = (29.5°, 3.8°)$, confidence intervals: 1σ: $-0.37° \rightarrow +0.28°$, 2σ: $-0.66° \rightarrow +0.56°$, 3σ: $-0.94° \rightarrow +0.84°$. The sky map containing the most likely COMPTEL/IPN position is shown in Figure 8.

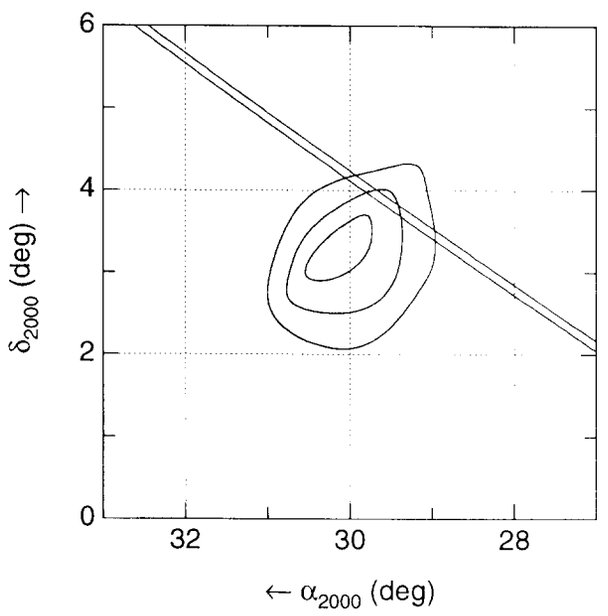

Fig. 8. Maximum likelihood sky map showing the most likely position of GRB 940217 using COMPTEL imaging and IPN triangulation. The contours denote confidence intervals of 1σ, 2σ, and 3σ, respectively. The burst position is at $(\alpha_{2000}, \delta_{2000}) = (29.5°, 3.8°)$.

3.4. "Post-burst" emission

During the entire burst emission (162 s) high energy photons (up to 4.4 GeV) were reported by the EGRET instrument (Hurley et al. 1994a, 1994c). Most importantly, on the subsequent orbit of CGRO, ~ 90 minutes later, EGRET detected 10 photons in its spark chamber – one with an energy of 18.4 GeV – within a 20 minute time interval from the burst region. In addition, the EGRET NaI calorimeter (TASC) detected during that "post-burst" interval (from $0^h\ 20^m$ to $0^h\ 40^m$ (UT) during TJD 9401) fluxes of $\sim 1.2 \times 10^{-3}$ and $\sim 1.4 \times 10^{-4}$ photons/(cm^2 s MeV) in the energy bands 1.07 – 6.1 MeV and 6.1 – 26.2 MeV, respectively (Hurley et al. 1994c).

During the CGRO orbit, subsequent to the event of GRB 940217, the "source" was visible to COMPTEL (i.e. within the FOV) on 1994 February 18 (TJD 9401), from 754 s (UT) until 3408 s (UT), a time interval which included the 20 minute interval of EGRET detection.

We have compared a time series of counts in "single detector mode" from both ranges (0.3 – 1.5 MeV and 0.6 – 10.0 MeV) accumulated during this "source visibility" period with data of same length accumulated 15 orbits ($\sim 8.4 \times 10^4$ s) later (i.e. representing a nearly identical orbital radiation environment). These datasets were subtracted from each other, any residual flux should indicate the presence of "post-burst" emission in the COMPTEL "single detector" energy range (0.3 – 10.0 MeV). During the "visibility" period of the source – i.e. the time interval corresponding to the positive EGRET detection of "post-burst" emission – we do not detect any significant signal in our 0.3 – 10.0 MeV data. The 2σ upper limits are 2.3×10^{-2} and 8.9×10^{-4} photons/(cm^2 s MeV) in the low range 0.3 – 1.5 MeV and high range 0.6 – 10.0 MeV, respectively.

Our method was cross-checked using a time interval during which the source was occulted (from 1994 February 17 (TJD 9400), 84900 s (UT) to 1994 February 18 (TJD 9401), 754 s (UT)) and again compared with data from a time interval of the same length, taken 15 orbits later. Subtraction of those datasets ("source occultation") resulted in residual counts compatible with zero.

"Double scatter mode" (telescope) data have also been searched for emission in the "post-burst" time interval (identical to the one as used by EGRET) by examining both the sky map (background subtracted events selected from a ~ 10° sky region around the burst position) and the lightcurve. We used a background estimate from a time series of events accumulated 15 orbits later. We did not find any significant excess in the lightcurve, and the derived image did not show any excesses above 2σ. The 2σ upper limits on the integrated flux in the 1.07 – 6.1 MeV and 6.1 – 26.2 MeV bands are 7.34×10^{-4} and 8.22×10^{-5} photons/(cm^2 s MeV), respectively.

In Figure 9 we compare our upper limits with the EGRET/TASC detections. We have also included in Fig-

ure 9 the best-fit power law to the EGRET (30 MeV – 30 GeV) spark chamber data extrapolated down to the COMPTEL energies (dashed line), and extreme ranges of this fit as given by the best-fit errors (dotted lines) (Hurley et al. 1994c). The best-fit power law shown is given[1] by $(1.03 \pm 0.4) \times 10^{-7} \times (\mathrm{E}/86\ \mathrm{MeV})^{-2.83\pm0.64}$ photons/(cm^2 s MeV).

We conclude that our COMPTEL upper limits are marginally consistent with the EGRET/TASC detections. All data (< 30 MeV) are consistent with the low energy extrapolation of the best-fit power law obtained for the EGRET spark chamber data (30 MeV – 30 GeV).

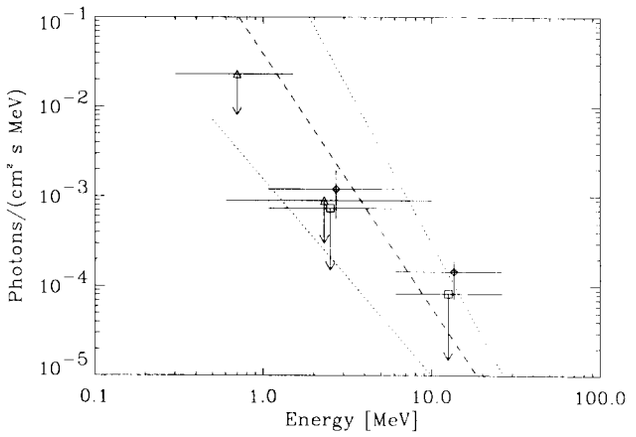

Fig. 9. "Post-burst" emission of GRB 940217. COMPTEL 2σ upper limits are shown ("single detector mode" = triangles, "double scatter mode" = squares) together with EGRET/TASC detections (diamonds and 1σ error bars) and the extrapolated best-fit power law to EGRET spark chamber data (30 MeV – 30 GeV, dashed and dotted lines). EGRET data are taken from Hurley et al. 1994c. See text for details.

4. Discussion

4.1. Spectral breaks

We have observed spectral breaks at around 1 MeV in most of the strong peaks of GRB 940217. In addition, the well known phenomenon of hard–to–soft evolution during MeV bursts (Norris et al. 1986, Winkler et al. 1992b, Schaefer et al. 1992a, Schaefer et al. 1992b, Hanlon et al. 1994) was again observed. The softening has been observed within peaks and also from peak to peak during the burst emission. Spectral breaks should be a diagnostic in the continuum of a photon spectrum, being related to optical depth effects in the MeV region. These breaks can be caused by several mechanisms including e^+e^- – pair creation from γ–γ interaction or from single photon interaction with strong (> 10^{12}G) magnetic fields, or photon splitting (see below).

4.2. Distance

A *lower limit* to the distance of GRB 940217 can be obtained by computing the angular offset ("parallax") from the IPN annulus at all COMPTEL sky bins and comparing each maximum likelihood ratio at each bin to the ratio obtained at the most likely COMPTEL/IPN position (Connors et al. 1993, Ryan et al. 1994). However, it is assumed that the offset of the most likely position from the IPN arc (Figure 8) of $\sim 0.5°$ reflects the experimental systematic error. We can further constrain our data by considering the fact that a "nearby" source can only result in an annulus with a true radius smaller than the one deduced from the IPN timing differences (which assumes a source at infinity). Using a Ulysses/CGRO distance of 3.038 AU and the IPN annulus radius of 69.33° centered on $(\alpha_{2000}, \delta_{2000}) = (21^h\ 54.9^m, +51°\ 57')$ at the time of the burst event (Hurley et al. 1994b), the significances of the IPN offsets have been evaluated and we derive a 2σ lower limit on the distance to GRB 940217 of 145 AU.

In order to derive an *upper limit* on the distance we use information on high energy emission together with temporal fine structure (following Ryan et al. 1994). Temporal fine structure has been described in Section 3.1 and the shortest peaks occur in peak #4 (see Figure 2) with a full width of ~ 0.1 s. This leads to a maximum size (2c×0.1s) of 6×10^4 km of the emitting site. Although EGRET reported energies (Hurley et al. 1994c) to be much higher, derivation of a distance limit requires information on temporal variations as provided only by COMPTEL. Concerning high energy emission, we observe during peak #4 a power law spectrum in the "single detector mode" data (6 s binning) with a break at 1 MeV indicating an opacity $\tau \sim 1$. However, the spectra obtained in both observing modes for peak #4 do not sharply cut off above 1 MeV and the power law spectrum (as observed in "double scatter mode") is not attenuated up to 4.4 MeV (> 3σ significance). Attenuation of the high energy flux (E > 1 MeV) should be expected if the burst source emits its radiation isotropically and homogeneously at large distances (Schmidt 1978) because of γ–γ interaction (e^+e^- – pair creation). Following Schmidt (1978) this leads to an upper limit on the distance of the homogenous and isotropic burst emitting site of 5.3 kpc using the break energy ($\sim$ 1 MeV) as an indicator for opacity $\tau \sim 1$ during peak #4. Using the highest significant (> 3σ) energy (4.4 MeV) of peak #4 as observed in the telescope spectrum, we obtain 1.3 kpc as limit of the distance to a homogenous isotropically radiating burst (site). For the full burst emission (162 s), the upper limit to the distance is 11.7 kpc (break energy $\sim$ 1 MeV).

[1] Note that the best-fit power law as given in the caption of Figure 3 of Hurley et al. (1994c) is erroneously too low by a factor of 10 (Hurley 1995, priv. communication).

If we consider beaming effects, however, the upper limit on the distance can be much larger. In fact, we can assume any cosmological distance and subsequently calculate how much beaming must be present at the source site in order not to see attenuation of high energy emission due to γ–γ interaction.

Using again peak #4 (slope = 2.63) and following Baring (1994, equation 15), we calculate a lower limit of the Lorentz beaming factor $\gamma_B = 27$ (for energy E = 4.4 MeV) and $\gamma_B = 18$ (1 MeV) for an assumed distance of 1 Gpc (z = 0.27).

Our observation of fast temporal variation at high (> 1 MeV) energies require a Lorentz factor of $\gamma_B > 18$. We conclude (following Baring 1994), that with such beaming, the cut–off energy for photon opacity is blue–shifted to $E \geq \gamma_B m_e c^2 = 9.2$ MeV to avoid Comptonization which is not observed in our data. Our observed spectral breaks are therefore too low in energy, which means that either GRB 940217 is closer than 1 Gpc, or the break is not produced by γ–γ interaction, but by a different process, e.g. single photon interaction with strong ($> 10^{12}$G) magnetic fields leading to pair creation, or photon splitting (cf. Baring 1990).

4.3. Lightcurve

Properties of extragalactic GRB's have been modelled recently in the frame of extragalactic radio sources using a precessing relativistic e^+e^- – beam with a Lorentz bulk factor of $\gamma_B \sim 10$ (Roland et al. 1994). These authors assume that the gamma–ray emission of the ejected e^+e^- – component has a non–thermal origin and is a product of e^+e^- – annihilation plus inverse–Compton losses. Anisotropic emission is a consequence of relativistic motion of the e^+e^- – component. Assuming that a compact object revolves around a central black hole at ~3 Schwarzschild radii, the perturbation beam model (Roland et al. 1994) predicts a typical time scale between peaks in the lightcurve of GRB's corresponding to the orbital rotation frequency of the compact object. From Figures 1 and 2, the typical time scale between peaks is seen to be of the order of 10 s, yielding a period of perturbation of the beam of a few 10^2 s and a central black hole mass of $\sim 10^4$ $M_\odot$. Gravitational interaction between the black hole and the revolving compact object would – according to this model – result in a perturbation of the accretion disk thereby inducing instabilities with a period of a few 10^2 s. Perturbation of the accretion disk will then produce a precession of the jet via its magnetic field lines, frozen in the plasma of the disk which might produce late events as seen by EGRET.

5. Conclusions

COMPTEL observations of GRB 940217 have shown that this event is very strong, complex, and long lasting. The burst consists of several peaks with short temporal fluctuations. Hard–to–soft spectral evolution has been observed throughout the burst event and also from peak to peak. The photon spectra obtained within the peaks can be modelled by single power law spectra and by broken power laws with break energies at around 1 MeV. No significant line emission is detected in any of the recorded spectra. Precise location of the event has been obtained through direct COMPTEL MeV imaging in combination with timing analysis by the Interplanetary Network. The COMPTEL upper limits obtained during the "post–burst" emission are marginally consistent with the detections as reported by EGRET. Distance limits to GRB 940217 have been derived assuming homogenous and isotropic emission as well as beamed emission. The lower limits obtained for the Lorentz beaming factor require that either the burst is closer than 1 Gpc, or that γ–γ interaction is not the mechanism responsible to produce spectral breaks.

Acknowledgements. We thank the BATSE team for the burst trigger, B. Dingus who provided us with the EGRET data prior to publication, and D. Band for the BATSE data. The COMPTEL project is supported by the German government through DARA grant 50 QV 9096, by NASA under contract NAS5–26645 and by the Netherlands Organisation for Scientific Research (NWO). K.S. O'Flaherty acknowledges receipt of a research fellowship from ESA. L.O. Hanlon acknowledges the Education Programme of the European Community for a fellowship and ESA/ESTEC for facilities.

References

Baring, M. 1990, MNRAS 244, 49
Baring, M. 1994, ApJS 90, 899
de Boer, H., Bennett, K., Bloemen, H. et al. 1992, in: Data Analysis in Astronomy IV (Eds.: Di Gesú, V. et al.), Plenum Press, New York, p. 241
Cash, W.C. 1976, ApJ 228, 939
Collmar, W., Bennett, K., Bloemen, H. et al. 1993, A&AS 97, 71
Connors, A., Aarts, H., Bennett, K. et al. 1993, A&AS 97, 75
Hanlon, L.O., Bennett, K., Collmar, W. et al. 1994, A&A 285, 161
Hurley, K., Boer, M., Niel, M. et al. 1994a, BAAS (184th Meeting of the AAS), paper 15.01
Hurley, K., Bertsch, D., Cline, T. et al. 1994b, IAUC 5940
Hurley, K., Dingus, B., Mukherjee, R. et al. 1994c, Nature 372, 652
Kippen, R.M., Macri, J., Ryan, J. et al. 1993, in: *Compton* Gamma–Ray Observatory (Eds. Friedlander, M., Gehrels, N., Macomb, D.), AIP Conf. Proc. 280, 823
Kippen, R.M., Macri, J., Ryan, J. et al. 1994a, IAUC 5937
Kippen, R.M., Connors, A., McConnell, M. et al. 1994b, 30th COSPAR meeting, in press
Lampton, M., Margon, B., and Bowyer, S. 1976, ApJ 208, 177
McNamara, B., Harrison, T., Ryan, J. et al. 1995: BAAS (185th Meeting of the AAS), paper 15.03
Norris, J., Share, G., Messina, D. et al. 1986, ApJ 301, 213
Roland, J., Frossati, G., and Teyssier, R. 1994, A&A 290, 364

Ryan, J., Bennett, K., Collmar, W. et al. 1994, ApJ 422, L67
Schaefer, B., Teegarden, B., Cline, T. et al. 1992a, ApJ 393, L51
Schaefer, B., Teegarden, B., Cline, T. et al. 1992b, in: Gamma-Ray Bursts (Eds.: Paciesas, W. & Fishman, G.), AIP Conf. Proc. 265, 180
Schmidt, W. 1978, Nature 271, 525
Schönfelder, V., Aarts, H., Bennett, K. et al. 1993, ApJS 86, 657
Varendorff, M.G., Bennett, K., de Boer, H. et al. 1992, in: Gamma-Ray Bursts (Eds.: Paciesas, W. & Fishman, G.), AIP Conf. Proc. 265, 77
Winkler, C., Bennett, K., Bloemen, H. et al. 1992a, A&A 255, L9
Winkler, C., Bennett, K., Hanlon, L. et al. 1992b, in: *Compton* Gamma-Ray Observatory (Eds. Friedlander, M., Gehrels, N., Macomb, D.), AIP Conf. Proc. 280, 845
Winkler, C., Bennett, K., Bloemen, H. et al. 1992c, in: Gamma-Ray Bursts (Eds. Paciesas, W. & Fishman, G.), AIP Conf. Proc. 265, 22

This article was processed by the author using Springer-Verlag LaTeX A&A style file *L-AA* version 3.